Aging and Disease
www.aginganddisease.org
Early access date: May 18, 2026
http://dx.doi.org/10.14336/AD.2026.0025

Original Article

Cellular Senescence in the Absence of Galactic Cosmic-Ray Muons

Àngela Llop-Hernández[1,2#], Júlia López[1,2#,a], Sara Verdura[1,2], Rebecca Hernández-Antolín[3], Laura Cid-Barrio[3], Carlos Peña-Garay[3,4], Tomás Alarcón[5,6,7*], Elisabet Cuyàs[1,2*], Javier A. Menendez[1,2*]

[1]Program Against Cancer Therapeutic Resistance (ProCURE), Catalan Institute of Oncology, 17007 Girona, Spain. [2]Metabolism and Cancer Group, Girona Biomedical Research Institute (IDIBGI), 17190 Salt, Girona, Spain. [3]Laboratorio Subterráneo de Canfranc, 22880 Canfranc-Estación, Huesca, Spain. [4]Institute for Integrative Systems Biology (I2SysBio), CSIC-Universitat de València, 46980 Paterna, Spain. [5]Centre de Recerca Matemàtica (CRM), 08193 Bellaterra, Barcelona, Spain. [6]ICREA, 08010 Barcelona, Spain. [7]Departament de Matemàtiques, Universitat Autònoma de Barcelona, 08193 Bellaterra, Barcelona, Spain

[Received January 8, 2026; Revised April 6, 2026; Accepted April 7, 2026]

ABSTRACT: Cellular senescence is a stress response that prevents the proliferation of damaged cells. As senescence has evolved in the near-surface biosphere, where cosmic background radiation (CBR) continuously delivers a low flux of highly penetrating muon particles, we investigated whether this persistent abiotic stress contributes to senescence thresholding. At the Canfranc Deep Underground Laboratory, an astrophysical facility located 800 meters beneath granite rock in the Spanish Pyrenees (~2,450 meters of water-equivalent depth), cosmic muons are suppressed by five orders of magnitude. There, we examined the senescence-induction dynamics in human cancer cells exposed to G0/G1- or G2/M-targeting chemotherapeutics and compared them to cells in adjacent, above-ground conditions with natural CBR. Muon depletion significantly reduced the acquisition of the senescence-associated β-gal-positive phenotype under conditions favoring a G0/G1 arrest with the CDK4/6 inhibitor palbociclib. SA-β-gal-positive states driven by G2/M arrest in response to the mitotic kinase inhibitor alisertib and the DNA-damaging radiomimetic bleomycin were insensitive to muon suppression. While the SENCAN classifier, which uses RNA-seq data to determine whether cell samples are senescent, and the senescence-associated secretory phenotype profiles were largely unaffected by the absence of cosmic-ray muons, muon depletion caused small variations at a transcriptome-wide level in the two pathways to senescence. Our hypothesis-generating study suggests that muons might act as abiotic signal-to-noise calibrators that facilitate the consolidation of senescence trajectories specifically associated with G0/G1 withdrawal. Our exploratory findings shed light on how life incorporated CBR evolutionarily to sense and respond to cellular damage, which could inform senescence operability in low-muon extraterrestrial habitats.

Keywords: Cosmic background radiation, deep-underground laboratory, cosmic silence, therapy-induced senescence, palbociclib, alisertib; bleomycin, Moon, Mars

INTRODUCTION

Cellular senescence is a pleiotropic cellular fate program with context-dependent consequences ranging from tissue repair and developmental morphogenesis to tumor suppression and chronic inflammation [1–7]. Senescence is also a hallmark of aging and age-related diseases [8–11]. It likely evolved from an ancient defense-repair module that emerged as a primordial DNA damage response (DDR) sensor and has been conserved from

***Correspondence should be addressed to:** Dr. Javier A. Menendez (Email: jmenendez@idibgi.org), Dr. Elisabet Cuyàs (Email: ecuyas@idibgi.org) and Dr. Tomás Alarcón (Email: talarcon@crm.cat), Girona Biomedical Research Institute, Edifici M2, Parc Hospitalari Martí i Julià, E-17190, Salt (Girona), Spain. #These authors contributed equally to this work. a: Current affiliation: Biochemistry and Molecular Biology Unit, Department of Biology, University of Girona, 17003 Girona, Spain.

Copyright: © 2026 Llop-Hernández A. et al. This is an open-access article distributed under the terms of the Creative Commons Attribution License, which permits unrestricted use, distribution, and reproduction in any medium, provided the original author and source are credited.

early eukaryotic cells to modern metazoans [12–17]. After multicellularity emerged, the module was augmented by a secretory signaling system that amplifies stress-induced and repair-coupled growth arrest in neighboring cells through the so-called senescence-associated secretory phenotype (SASP). This system also enables the recruitment of immune effectors to facilitate the clearance of damaged cells [18–21]. Accordingly, diverse forms of SASP are detectable across metazoan phyla, reflecting the ancestral "damage-broadcast" role of senescence [22–26].

Over evolutionary time, the primordial stress-adaptive senescence module has undergone multiple repurposings and exaptations. Its original function as a unicellular repair system evolved into a multifaceted program that protects the architecture and homeostasis of tissues in multicellular organisms [27–31]. Senescent cells limit neoplastic transformation by halting the proliferation of damaged, premalignant cells and by undergoing immune-mediated elimination [22–35]. Transient senescence also supports tissue repair by coordinating wound resolution, matrix remodeling, and angiogenesis [36–42]. During vertebrate development, programmed waves of senescence shape morphogen gradients, refine morphogenesis, and cooperate with apoptosis to sculpt embryonic structures [43–45]. Senescence signals can destabilize differentiated states to promote regenerative plasticity, as observed in cnidarians and urodele amphibians [24,46–49], although this property is largely suppressed in complex bilaterians [50–54]. In mammals, the accumulation of senescent cells drives chronic inflammation, cancer, and age-related pathologies [55–59], reflecting an evolutionary trade-off between regenerative plasticity and the necessity of genomic stability in complex organisms.

Senescence is triggered by various sublethal insults, including viral infection, oncogenic stress, oxidative bursts, telomere erosion, and ionizing radiation, among others [60–67]. Interestingly, terrestrial life has continuously endured and adapted to a continuous, global source of sublethal genotoxic damage in the form of the steady flux of cosmic background radiation (CBR). Geological evidence suggests that organisms have experienced comparable or greater CBR fluxes for nearly four billion years, with increased exposure during solar minima and geomagnetic inversions [68, 69]. CBR delivers a relentless flux of highly charged decay products resulting from cosmic ray collisions with atmospheric particles, called muons, which constitute ~75% of the sea-level dose rate. These highly penetrating particles can induce single-strand breaks (SSBs), oxidative lesions, and occasional clustered double-strand breaks (DSBs) in exposed genomes [70–75]. This constitutive, low-level chronic stress may have influenced the evolution of primordial senescence modules by sensitizing cells to a rapid defense response to prevent the propagation and accumulation of damaged cells. To test the hypothesis that senescence commitment might be calibrated radiobiologically to the baseline level of unavoidable background radiation, we must study senescence phenomena in environments depleted of muons. This ultra-low CBR condition is known as "cosmic silence".

Deep underground laboratories (DULs) provide a near-zero CBR environment, enabling the formal study of how the physics of Earth's radiation impacts cell biology. These facilities were originally designed for the study of rare-event astrophysics, including proton decay, neutrino interactions, and dark matter searches. Recently, the research carried out in DULs has expanded into new fields, particularly at the intersection of cell biology and radiobiology [76–78]. The *Laboratorio Subterráneo de Canfranc* (LSC), the second-largest DUL facility in Europe and one of 14 operational DULs worldwide, is located 800 meters beneath the Spanish Pyrenees granite (Fig. 1A). The LSC provides shielding equivalent to ~2,450 meters of water, reducing muon flux by nearly five orders of magnitude (Fig. 1B) [79,80]. We took advantage of the recently developed LSC Biology Platform to investigate the effects of muon depletion on therapy-induced senescence (TIS) phenomena for the first time [81–88]. We replicated TIS experiments under the same conditions simultaneously in two laboratories with identical features: one deep underground and the other equally elevated above ground (AGL) and unshielded with natural CBR exposure. The only difference was the nearly complete suppression of muon flux inside the DUL. A variety of mechanistically diverse senescence-inducing agents engaging different cell cycle arrest trajectories, namely, the G0/G1 arrest promoter palbociclib and the G2/M arrest promoters alisertib and bleomycin, were applied to A549 human lung epithelial cells. Senescence readouts included quantification of senescence-associated β-galactosidase activity (SA-β-gal$^+$), scoring of senescence predictors based on RNA-seq data [89], examination of the coding transcriptome, and multiplex profiling of SASP composition [90,91].

Our exploratory study provides hypothesis-generating evidence that muon-less cosmic silence might prevent the commitment and consolidation of the SA-β-gal$^+$ senescence type (or senotype) driven by G0/G1-related cell cycle withdrawal. However, extrinsic cosmogenic noise has a negligible effect on SA-β-gal+ commitment in senotypes that undergo cell cycle withdrawal via the G2/M pathway. These results suggest an unexpected mechanistic role for cosmogenic radiation in calibrating the signal-to-noise threshold that determines the deepening progression of senescence, depending on the stressor trajectory of cell cycle withdrawal. This pilot study provides new insights into how radiobiological

physics on Earth may have influenced the evolution of damage-containment senescence programs. The study also generates testable predictions about how senescence could respond to different stresses in muon-depleted extraterrestrial habitats, such as the Moon and the undersurface of Mars.

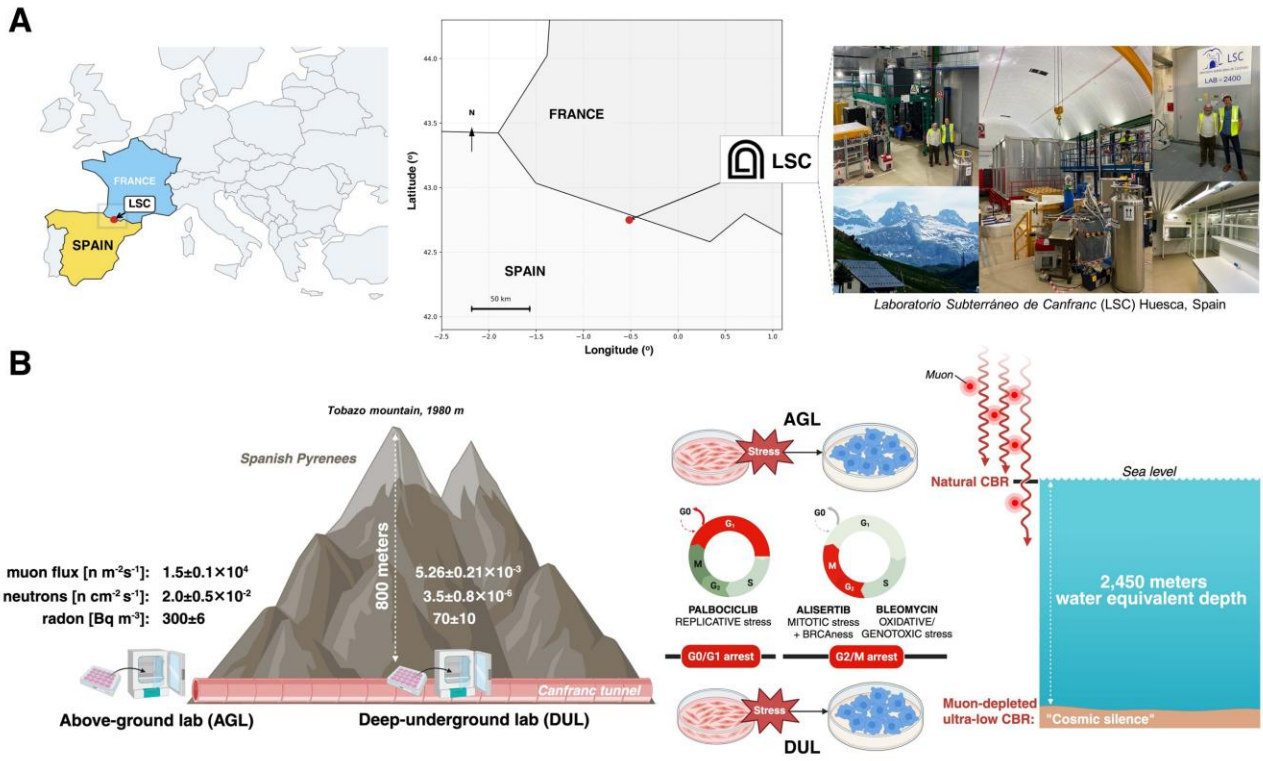

Figure 1. Radiobiological conditions and conceptual framework for studying cellular senescence in cosmic silence. (A) Geographical location and representative views of the Laboratorio Subterráneo de Canfranc (LSC) in Huesca, Spain, situated in the central Spanish Pyrenees near the Spanish-French border. The European locator, regional map, and photographs of the facility identify the deep-underground laboratory used in this study. *Bottom left.* Radiobiological comparison between the above-ground laboratory (AGL) and the deep-underground laboratory (DUL) facilities at the LSC Biology platform. The DUL facility of the Canfranc Biology Platform is located 800 meters beneath the granite of the Tobazo mountain. Compared to the AGL environment, the DUL significantly reduces the cosmic background radiation (CBR) field, including cosmic-ray muon flux, neutrons, and radon. Similar environmental conditions in the AGL and DUL facilities (see **Fig. 2**) and the use of identical, matched incubators ensure consistent culture conditions (temperature, humidity, and gas exchange). This creates a controlled, radiobiologically distinct platform suitable for studying the influence of muon depletion on the execution of senescence programs. **(B)** Conceptual framework of the study. At sea level, cells are continuously exposed to a natural CBR environment, dominated by secondary muons. At the LSC-DUL depth, which provides 2,450 meters of water-equivalent shielding, the muon flux is nearly abolished, generating an ultra-low CBR condition referred to as "cosmic silence." Using matched cell-culture conditions in the AGL and DUL facilities, we tested how natural versus muon-depleted CBR environments influence therapy-induced senescence (TIS) phenomena triggered by the G0/G1-targeting stressor palbociclib and the G2/M-targeting stressors alisertib and bleomycin.

MATERIALS and METHODS

Reduction of cosmic ray muon fluxes in the LSC-DUL

Primary cosmic rays produce a mixed field of penetrating relativistic muons ($1.5\pm0.1\times10^{4}$ m^{-2} s^{-1}) and spallation neutrons ($2.0\pm0.5\times10^{-2}$ cm^{2} s^{-1}) at sea level (Fig. 1B). Together with γ-rays, these particles contribute ~0.26 mSv per year to the natural radiation dose received by the near-surface Earth's biosphere. The LSC-DUL is the Spanish national hub for low radioactivity techniques and their associated scientific and technological applications [79–81]. Located in an unused railway tunnel connecting Spain and France under Monte Tobazo in the Pyrenees, the LSC-DUL passively attenuates CBR by up to five orders of magnitude. This achieves an ultra-low-dose background irradiation in the sub-millisievert range. Specifically, the natural rock shielding of the LSC-DUL is equivalent to 2,450 meters of water, yielding residual fluxes of $5.3\pm0.21\times10^{-3}$ cm^{-2} s^{-1} muons, 1.23±0.17 cm^{-2} s^{-1} γ-rays, and $3.5\pm0.08\times10^{-6}$ cm^{-2} s^{-1} neutrons ([78–81,92,93]; Fig. 1B). The environmental concentration of radon, the main source of natural radiation in underground facilities, is 60–100 Bq/m^{3} (approximately one-third of

surface levels). Forced ventilation using a Radon Abatement System (RAS) reduces the airborne radon concentration further to ≈1 mBq/m^3 in the LSC-DUL atmosphere (79). During the nine-day acclimation period (and thereafter), environmental dose rates of integrated muon flux, thermal neutron background, and radon activity were monitored using plastic scintillators, a ^{3}He proportional counter (neutrons), and AlphaGuard detectors, respectively [79,93]. Temperature and humidity parameters measured in AGL and DUL facilities confirmed environmental stability across sites during the study period from November to December 2023; Fig. 2A). Only radon (^{222}Rn) activity decreased significantly underground (~70 Bq m^3) compared to the AGL (~350 Bq m^{-3}).

Cell lines and culture

The human cell line A549 (ATCC CCL-185) was obtained from the ATCC (Manassas, VA, USA) and routinely expanded in Dulbecco's modified Eagle's medium (DMEM, Gibco), which was supplemented with 10% heat-inactivated fetal bovine serum (FBS), 1% L-glutamine, 1% sodium pyruvate, 50 IU/mL penicillin, and 50 µg/mL streptomycin. Cells were authenticated by STR profiling, both performed by the manufacturer and confirmed in-house at the time of purchase according to ATCC guidelines. The cell lines were screened for mycoplasma contamination using a PCR-based method for *Mycoplasma* detection prior to experimentation and were tested intermittently thereafter.

Cells were routinely grown at 37°C in a humidified atmosphere containing 5% CO_2 and were in the logarithmic growth phase at the start of the experiments. Standard cell culture parameters, such as temperature, oxygen/carbon dioxide levels, and humidity, were measured and cross-calibrated in identical ICO150 incubators (Memmert GmbH + Co.KG, Germany) located in the DUL and the adjacent above-ground laboratory (AGL). The AGL is situated 200 m from the DUL tunnel portal at the same altitude (□1,390 m above sea level) as the DUL.

Drugs

PD-0332991/palbociclib (Cat. #S1116) was purchased from Selleckchem (Houston, TX, USA). MLN8237/alisertib (Cat. #331-10890-1) and bleomycin sulfate (Cat. #331-11727-3) were purchased from RayBiotech Inc. (Norcross, GA, USA).

Therapy-induced senescence (TIS)

Nine days before initiating therapy-induced senescence (TIS) experiments, early-passage cells were trypsinized, counted using Trypan Blue exclusion (<3% dead cells), and seeded into matched T75 flasks. Half of the flasks were kept on the surface LSC-AGL, and the other half were transported by van (<25 minutes) to the Biology Platform at the LSC-DUL inside the tunnel (Fig. 2B). Both cohorts were maintained for nine days to allow equilibration to the respective radiation backgrounds.

Cells were seeded in 150-mm dishes for 24 h before treatment with palbociclib (1 and 5 µmol/L), bleomycin (5 and 20 µmol/L), or alisertib (100 and 500 nmol/L) strictly in parallel at the LSC-AGL and LSC-DUL facilities for up to 7 days. Untreated (proliferative) controls were seeded also in 150-mm dishes and cultured in parallel for up to 7 days. The dynamics of AGL vs. DUL TIS phenotypes were described by monitoring the number and timing of SA-β-gal staining, mRNA-Seq (coding transcriptome) signatures, and SASP composition, as indicated in Figure 2B. Cell supernatants (for ulterior secretome analyses) and whole cell lysates (for ulterior RNA isolation and RNA-seq analyses) were collected from cell cultures, and stored at –80 ºC until used. After 3 and 7 days, quantification of senescence-associated β-galactosidase (SA-β-gal)-positive cells was performed using the immunohistochemistry-based, semi-quantitative Senescence β-Galactosidase Staining Kit (see below).

Cumulative population doubling (CPD) level

The growth of A549 cells was profiled by calculating their CPD levels. The cells were counted at seeding and harvesting, and their CPD levels were calculated using the following equation:

$$CPD = [Log_{10}(N_H) – Log_{10}(N_I)/Log_{10}(2)]$$

Where N_I is the initial cell number at seeding and N_H is the cell number at harvest. The CPDL was obtained by adding the doubling levels from each harvest to the previous one. Cultivation was continuous from day 1 to day 7 after treatments with vehicle, palbociclib, alisertib, and bleomycin, with harvesting on days 1, 3, 5, and 7.

Senescence-associated β-galactosidase activity (SA-β-Gal) staining

Cellular β-galactosidase activity was detected using the Senescence β-Galactosidase Staining Kit (Cat. #9860, Cell Signaling Technology, Danvers, MA, USA) according to the manufacturer's instructions. To quantitatively assess the induction of SA-β-gal-positive senescent states, cells were seeded into six-well plates and

treated with senescence inducers without refreshing the drug before SA-β-gal staining was performed on days 0, 3 and 7. The total number of SA-β-gal-positive cells was quantified by manual counting from at least five images per well from the same biological replicate in triplicate, with at least 2,000 cells were counted per condition.

RNA sequencing (RNA-seq) analysis

Total RNA was extracted from cells using the RNA Plus Kit (Macherey-Nagel, Germany) following the manufacturer's instructions. The RNA-seq and bioinformatics analyses were outsourced to Macrogen Inc (Republic of Korea). Briefly, RNA-seq libraries were prepared using the Illumina® TruSeq® Stranded Total RNA Sample Preparation Kit (Illumina, Inc., San Diego, USA) according to the manufacturer's recommendations. Samples were sequenced on the NovaSeq 6000 system from Illumina using 2 x 150 bp paired-end reads. The reads were aligned to the human reference genome GRCh37 using HISAT2 (v2.1.0) [94], and transcript assembly was performed using StringTie (v2.1.3b) [95]. Differentially expressed gene (DEG) analysis was performed on comparative pairs using DESeq2 [96]. Senescence scores were calculated using the SENCAN elastic net classifier (n=137 genes) on the processed RNA sequencing data of the untreated proliferative controls and TIS phenotypes. The available script can be found at https://ccb.nki.nl/publications/cancer-senescence/.

Gene set enrichment analyses

We performed a gene set enrichment analysis (GSEA) was performed using GenePattern with gene sets from the Molecular Signatures Database (MSigDB), including those related to "Hallmark" and "DNA damage–related" pathways. Normalized enrichment scores (NES) were used for downstream analyses and visualization. To provide an overview of pathway activity across all conditions, we considered only pathways with an FDR ≤ 0.2, representing NES values as heatmaps. Pathways were further selected based on both, enrichment magnitude. Specifically, we selected pathways pathways showing |NES| ≥ 1.5 in at least one comparison and significant enrichment (FDR ≤ 0.2) were selected. Heatmaps were generated using the R package *pheatmap*.

Enrichment analysis was performed also using the g:Profiler tool (https://biit.cs.ut.ee/grolifer/) with the significant DEG list based on the Gene Ontology (GO) database [97]. The g:Profiler tool performs statistical enrichment analysis to detect the overrepresentation of information from GO terms, biological pathways, regulatory DNA elements, human disease gene annotations, and protein-protein interaction networks. The web-based gene set enrichment analysis platform, Enrichr [98], was used to analyze the enrichment of genes that were either commonly upregulated or downregulated after treatment with TIS stressors.

Secretome

The qualitative and quantitative composition of TIS-associated secretomes in terms of cytokines, chemokines, and growth factors was characterized using Luminex® multiplex bead-based immunoassays. Briefly, cell culture supernatants from non-senescent (proliferative controls) and cancer cells that were made senescent with mechanistically different TIS inducers, as described above, were collected at days 3, 5 and 7 in strict parallel. The collected extracellular milieus were sent to a third-party commercial laboratory (Eve Technologies, Canada) to perform the Cytokine/Chemokine 96-Plex Discovery Assay® Array (HD96). Multiplex cytokine/chemokine data were normalized by cell number.

Statistical Analysis

All cell-based observations were confirmed by at least two independent biological experiments, each performed in technical triplicates for every cell line and for each condition. Bar graphs, curves, and statistical analyses were generated using GraphPad Prism 10 (GraphPad Software, San Diego, CA). The statistical significance of the differences in SA-β-gal+ scores was measured using the non-parametric Mann-Whitney U Test (two groups) and are presented for exploratory comparison. *P*-values from multiple comparisons across outcome measures in RNA-seq analyses were adjusted via the Benjamini-Hochberg (BH) false discovery rate procedure. Data are expressed as mean ± SD or 95% confidence intervals, and statistical significance was defined as p values < 0.05.

RESULTS

The A549 cell line originates from the type II epithelium of human alveoli. Therefore, its stress responses resemble those of the lung compartment, in which age-related senescence can lead to fibrosis, chronic obstructive pulmonary disease, and cancer. The A549 cell line carries wild-type *TP53* and an operative p53-p21-p38/RB signaling pathway. This allows researchers to study how radiation [99], various chemotherapeutic agents [100,101], viral infection [60], and even cigarette smoke extract [102] induce robust senescence hallmarks, such as SA-β-gal, DDR foci, and SASP. These studies have also enabled the development and training of omic resources, such as the SENESCopedia dataset, as well as machine-

learning classifiers for senescence, such as SENESCAN [89]. A549 cells have become the reference cell model for rapid and reproducible TIS protocols; therefore, we chose them to investigate the impact of environmental depletion of cosmic ray muon particles impacts on the execution, kinetics, and molecular processes underlying senescence-induction trajectories driven by either G0/G1- or G2/M paths-to-arrest.

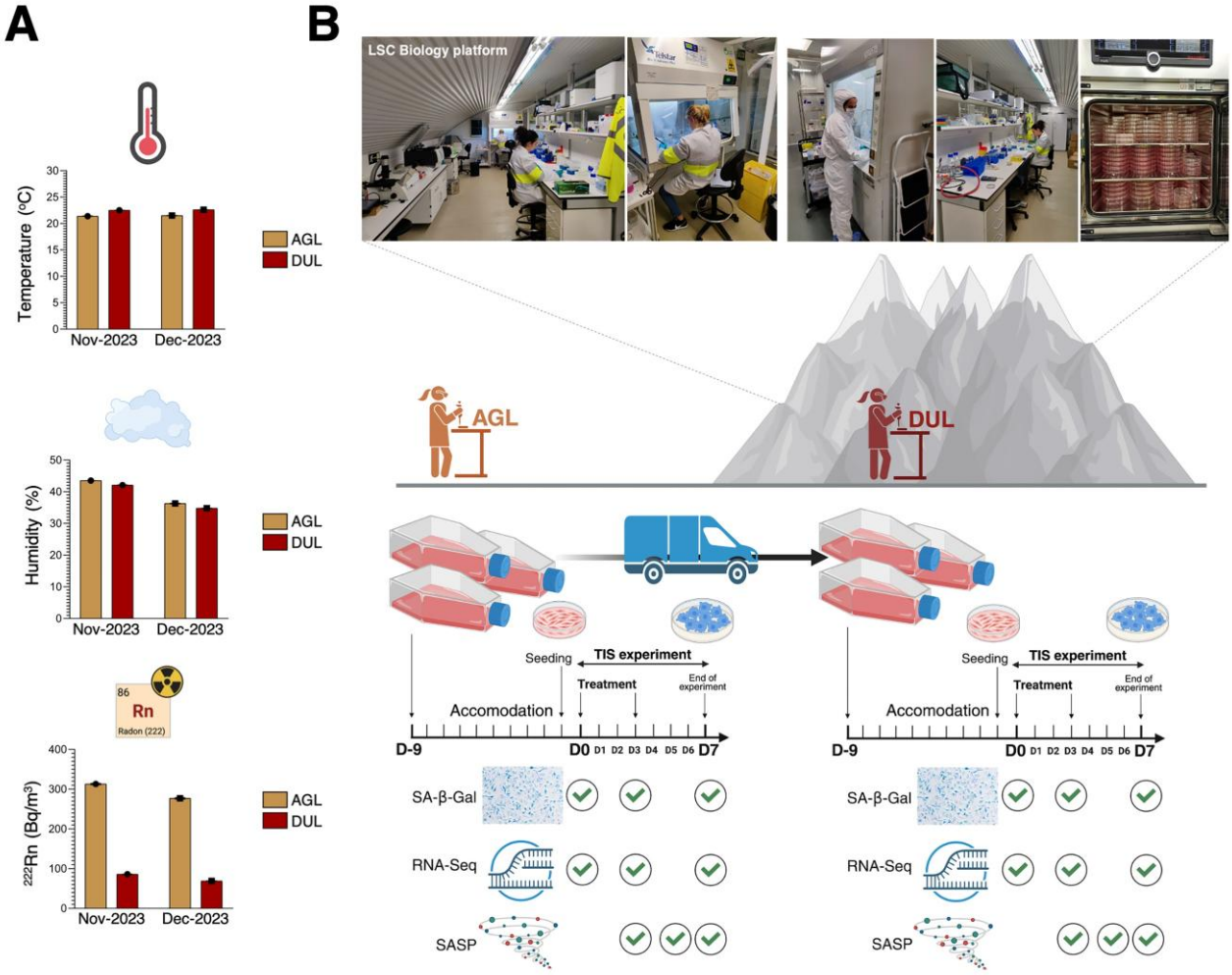

Figure 2. Experimental design and environmental characterization of the LSC Biology Platform. (A) *Environmental monitoring.* From November to December 2023, temperature, relative humidity, and radon (^{222}Rn) levels were continuously logged in the AGL and DUL facilities throughout the experimental period. (DUL: November 2023, number of measures = 4,319; December 2023, number of measures = 4,462; AGL: November 2023, number of measures = 4,320; December 2023, number of measures = 3,700; Columns represent the arithmetic mean, and error bars the uncertainty of the mean). **(B)** *Experimental logistics.* Parallel biological replicates of A549 human epithelial cancer cells were seeded and pre-acclimated for nine days in each environment before treatment initiation (day 0). Samples for senescence-associated β-galactosidase (SA-β-gal) staining, RNA sequencing (RNA-seq) for transcriptomic analysis, and senescence-associated secretory phenotype (SASP) profiling were collected at defined sampling time points (green checkmarks). This design ensured synchronized temporal sampling under rigorously monitored environmental conditions, isolating the effects of ambient cosmic radiation depletion on TIS dynamics. *Right.*

On day 0, nine days after the cell cultures were exposed to their respective radiation LSC-AGL/LSC-DUL backgrounds, three mechanistically distinct senescence triggers were applied simultaneously to A549 cell cultures in the AGL and DUL facilities (Fig. 2). These triggers included two graded concentrations of palbociclib (1 and 5 µmol/L), which targets the G0/G1 pathway, and two G2/M pathway-targeting stressors: alisertib (100 and 500 nmol/L) and bleomycin (5 and 20 µmol/L), Palbociclib, a selective inhibitor of cyclin-dependent kinases 4 and 6 (CDK4/6), induces senescence via replicative stress [91,103]. Alisertib (MLN8237) is an Aurora A kinase inhibitor that not only induces mitotic stress but also mimics "BRCAness" by causing defects in homologous DNA recombination repair and double-strand breaks [104–107]. Bleomycin, an antibiotic, promotes oxidative stress by generating free radicals, induces genotoxic stress via single- and double-strand

breaks in DNA, and has been used to model space radiation due its radiomimetic properties [108–111].

Due to significant logistical, temporal, and operational limitations associated with conducting biological experiments performed in an astrophysical DUL, we are now reporting on a two-biological-replicate campaign conducted from November to December 2023. This campaign was intentionally designed as an exploratory study. It was designed to generate hypotheses, capture robust effect tendencies, and demonstrate feasibility. It was not designed to provide definitive statistical inferences. This campaign was preceded by a three-week technical optimization phase, during which key experimental parameters, including cell seeding density, culture plate format, and related assay conditions, were adjusted before launching the final biological replicate series.

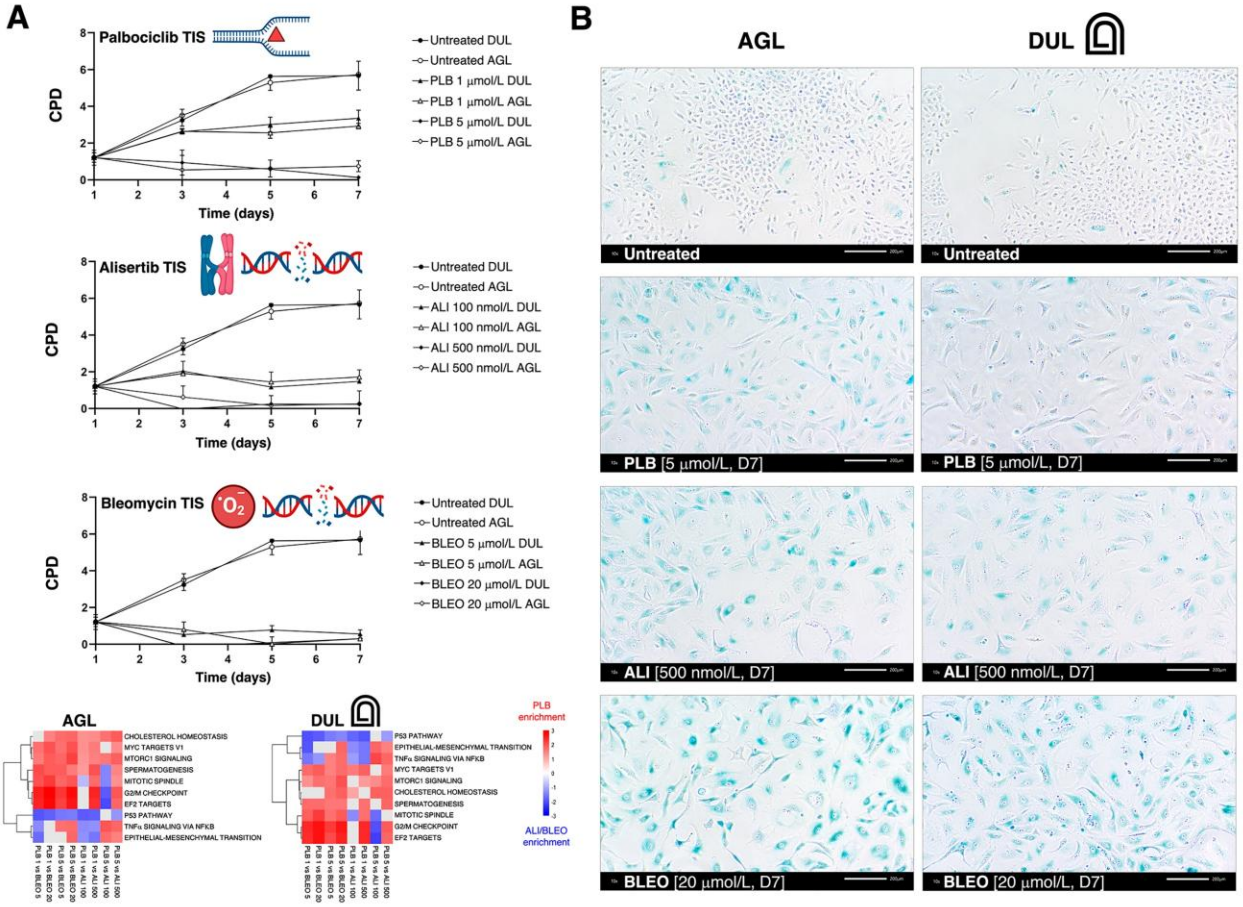

Figure 3. Cosmic silence preserves growth arrest in response to chemotherapy but selectively attenuates palbociclib-associated senescence features. (A) *Top.* Cumulative population doubling (CPD) of A549 cells cultured in the LSC above-ground laboratory (AGL) o deep-underground laboratory over 7-days of continuous exposure to palbociclib (1 or 5 µmol/L), alisertib (100 or 500 nmol/L) or bleomycin (5 or 20 µmol/L). The data represent the mean number of CPDs obtained from two individual preparations of A549 cell cultures over seven days of culture, with or without graded concentrations of palbociclib, alisertib, or bleomycin. Error bars show the SD of the mean, but they are not visible at some points because they are within the field of the symbols. *Bottom.* RNA-seq–based pairwise GSEA of Hallmark gene sets was performed between palbociclib-induced senescent transcriptomes and those generated by alisertib or bleomycin in AGL and DUL conditions (n=2 independent biological replicates). Heatmaps show significantly enriched signatures passing the indicated thresholds (FDR ≤ 0.2; |NES| ≥ 1.5), with red denoting relative enrichment in palbociclib TIS and blue denoting relative enrichment in alisertib/bleomycin TIS. **(B)** Representative bright-field/SA-β-gal staining microphotographs of untreated, proliferative control cells and cells exposed to the highest dose of each inducer (palbociclib, 5 µmol/L; alisertib, 500 nmol/L; and bleomycin, 20 µmol/L) for 7 days in AGL and DUL cultures (n=2 independent biological replicates; n≥3 technical replicates for each condition). All treatments induced characteristic senescence-associated cytomorphological remodeling, as detailed explanation in the Results section, together with SA-β-gal positivity consistent with lysosomal alkalinization and expansion. Scale bars, 200 µm.

Loss of proliferative capacity in response to chemotherapeutic is unaffected by cosmic silence.

Direct cell-cycle profiling and immunoblot-based arrest markers were not incorporated into the synchronized LSC-AGL/LSC-DUL campaign. However, the senescence-induction regimen used was not exploratory but rather a senescence platform previously validated in our laboratory. In companion studies conducted simultaneously with the current LSC underground study [101,112], we benchmarked the same A549 model using the same 7-day, no-drug-refreshment TIS protocol and the highest inducer dose as in the LSC-DUL study. Under these matched conditions, the A549 cells exhibited a consistent complete loss of retinoblastoma (RB) phosphorylation at Ser807/811. This robust marker of senescence-associated proliferative arrest reflects the restoration of the growth-suppressive RB state and repression of cell-cycle progression, rather than a transient reduction in proliferation. This was accompanied by a marked redistribution of the cell-cycle profile (G1 arrest in response to palbociclib and G2/M arrest in response to alisertib and bleomycin), reduced PCNA (proliferating cell nuclear antigen) expression and accumulation of $p21^{WAF1/Cip1}$. These traits are all consistent with the establishment of a *bona fide* senescent state [101,112].

To confirm the loss of proliferative capacity in response to senescence stressors in both muon-replete AGL and muon-deplete DUL environments, we measured the cumulative population doubling (CPD) levels of A549 cells in response to graded concentrations of palbociclib, alisertib, and bleomycin (Fig. 3A, *top panels*). Untreated cells in both AGL and DUL cultures exhibited an increase in CPDs, reaching ~5.5-6.0 by day 7. All senescence-inducing treatments reduced proliferative capacity in a clear dose-dependent manner. Alisertib and bleomycin were particularly effective, even at the lower doses tested, whereas higher doses of palbociclib, alisertib, and bleomycin caused complete growth arrest. The sole exception was low-dose palbociclib (1 μmol/L), which still allowed residual proliferation in both AGL and DUL environments (Fig. 3A, *top panels*). The loss of proliferative capacity, a defining hallmark of cellular senescence, was not significantly altered under muon-depleted conditions.

Consistent with the CPD data, when TIS cancer cells in the AGL and DUL environments were pairwise compared using mRNA-focused transcriptome sequencing (mRNA-seq) profiles (Hallmark sets, FDR ≤ 0.2, NES ≥ 1.5), it was found that palbociclib-induced senescent populations retained relatively stronger enrichment of programs associated with proliferation (MYC/E2F targets, mTORC1 signaling) and, in several contrasts, G2/M checkpoint-related features, in both AGL and DUL environments (Fig. 3A, *bottom panels*). Conversely, p53 pathway signatures were more prominently enriched in alisertib- and bleomycin-induced senescent states, consistent with a more consolidated stress-response program. Notably, alisertib also exhibited stronger relative engagement of mitotic spindle and G2/M checkpoint hallmarks, consistent with its mechanism of action and deeper mitotic-arrest-derived senescence endpoint. Together, these heatmaps suggest that palbociclib-induced senescence is comparatively shallower and more permissive to residual proliferation, while alisertib- and bleomycin-induced senescence occupy a more stable, deeper arrest state.

Cosmic silence reduces the number of SA-β-gal-positive senescent cells induced by palbociclib

All of the TIS stressors promoted the appearance of the characteristic senescence-associated cytomorphological remodeling, including an enlarged, hypertrophic, and flattened cytomegalic phenotype (Fig. 3B). Bleomycin and alisertib, as well as palbociclib to a lesser extent, promoted the appearance of a large number of cytoplasmic granularities as well as enlarged irregularly shaped nuclei and grape-like, multinuclear clusters. These are hallmarks of senescence-like cells. Bleomycin-induced senescent cancer cells exhibited more cytoplasmic protrusions and fewer contacts with neighboring cells. The expansion and acidification dysfunction (alkalinization) of the lysosomal compartment, a phenotypic and functional hallmark of late, hard-locked senescent states that can be measured by cytochemically detecting SA-β-galactosidase (SA-β-gal) activity [113–115], was also confirmed. At a first glance, DUL versus AGL environmental conditions did not appear to greatly impact the establishment of bleomycin- and alisertib-driven senescent phenotypes. However, it was noteworthy that the number of cells exhibiting the senescence-associated cytomorphological and functional remodeling characteristic of the senescent phenotype, and particularly the acquisition of SA-β-gal positivity, seemed to be notably lower when A549 cells were exposed to palbociclib under DUL conditions than under AGL conditions (Fig. 3B).

To better assess the impact of muon depletion on the dynamics of SA-β-gal+ cells in response to G0/G1- or G2/M-targeting stressors, we arbitrarily defined early and late senescence stages based on the time elapsed from the onset of stress induction: three days for early senescence and seven days for late senescence. The DUL environment reduced the ability of a low dose of palbociclib (1 μmol/L) to induce late-stage SA-β-gal-positive senescent phenotypes the by more than 2-fold

(Fig. 4). Though less pronounced, the ability of a high concentration of palbociclib (5 μmol/L) to promote the appearance of SA-β-gal-positive senescent cells was also significantly decreased in the DUL environment at both the early and late stages (Fig. 4).

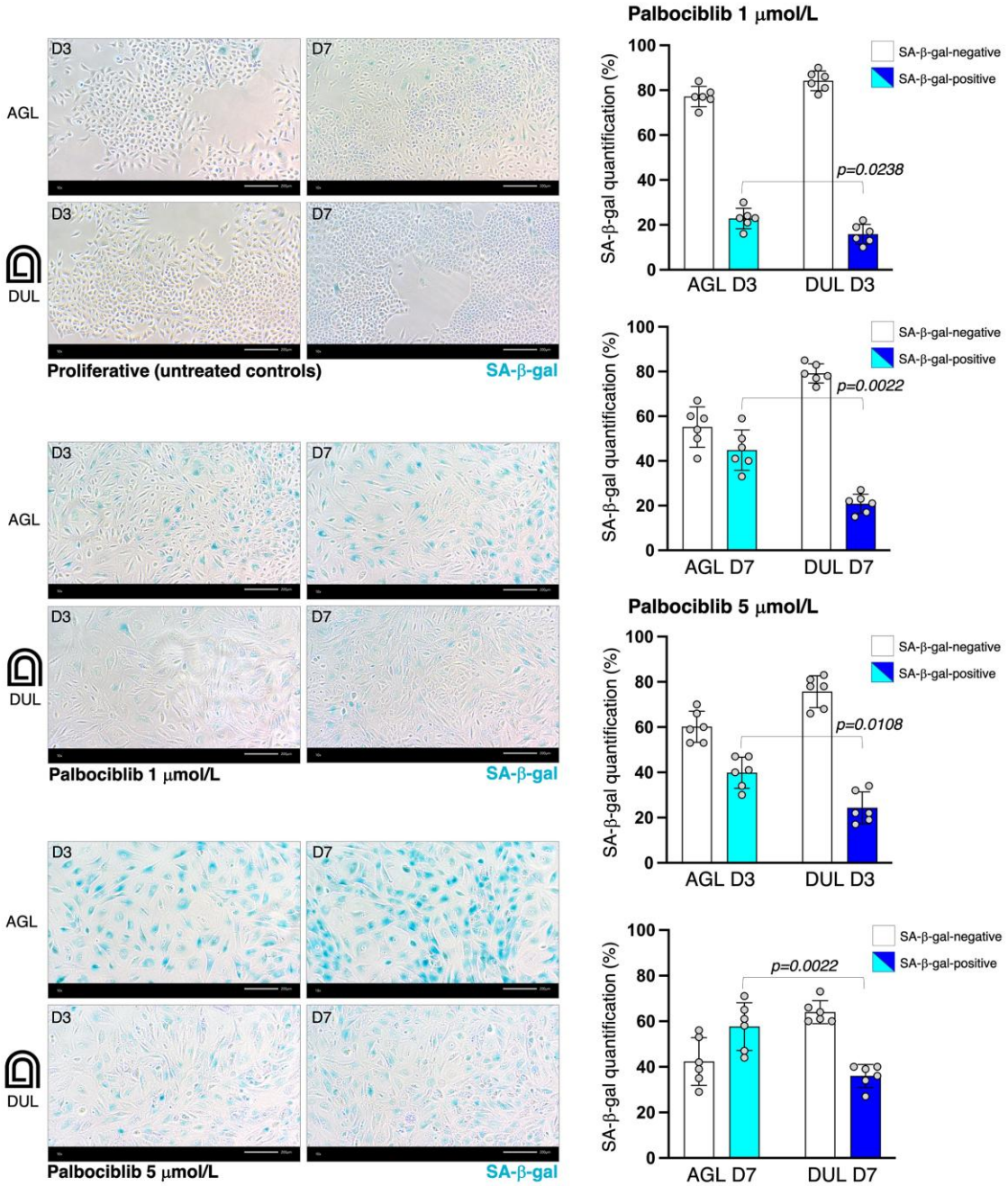

Figure 4. Cosmic silence attenuates the induction kinetics of palbociclib-triggered SA-β-gal-positive senescent states. This figure provides a quantitative assessment of senescence-associated β-galactosidase (SA-β-gal) activity in A549 cells exposed to low- and high-dose palbociclib (1 and 5 μmol/L) under standard (above-ground laboratory, AGL) and muon-depleted (deep-underground, DUL) radiobiological conditions. The cells were pre-acclimated for nine days to their respective environments before treatment and analyzed at the early (day 3, D3) and late (day 7, D7) stages of therapy-induced senescence. *Left panels.* Representative microphotographs illustrate the extent of SA-β-gal-positivity commonly associated with lysosomal expansion occurring in senescent cells. Scale bars, 200 μm. *Right panels.* Quantification of at least 2,000 cells per condition is shown as a percentage of SA-β-gal-negative (white) and SA-β-gal-positive (blue) cells. Data represent the mean ± S.D. (n=2 independent biological replicates; n≥3 technical replicates for each condition). *p* values shown were calculated using a two-sided non-parametric Mann–Whitney U test and are presented for exploratory comparison.

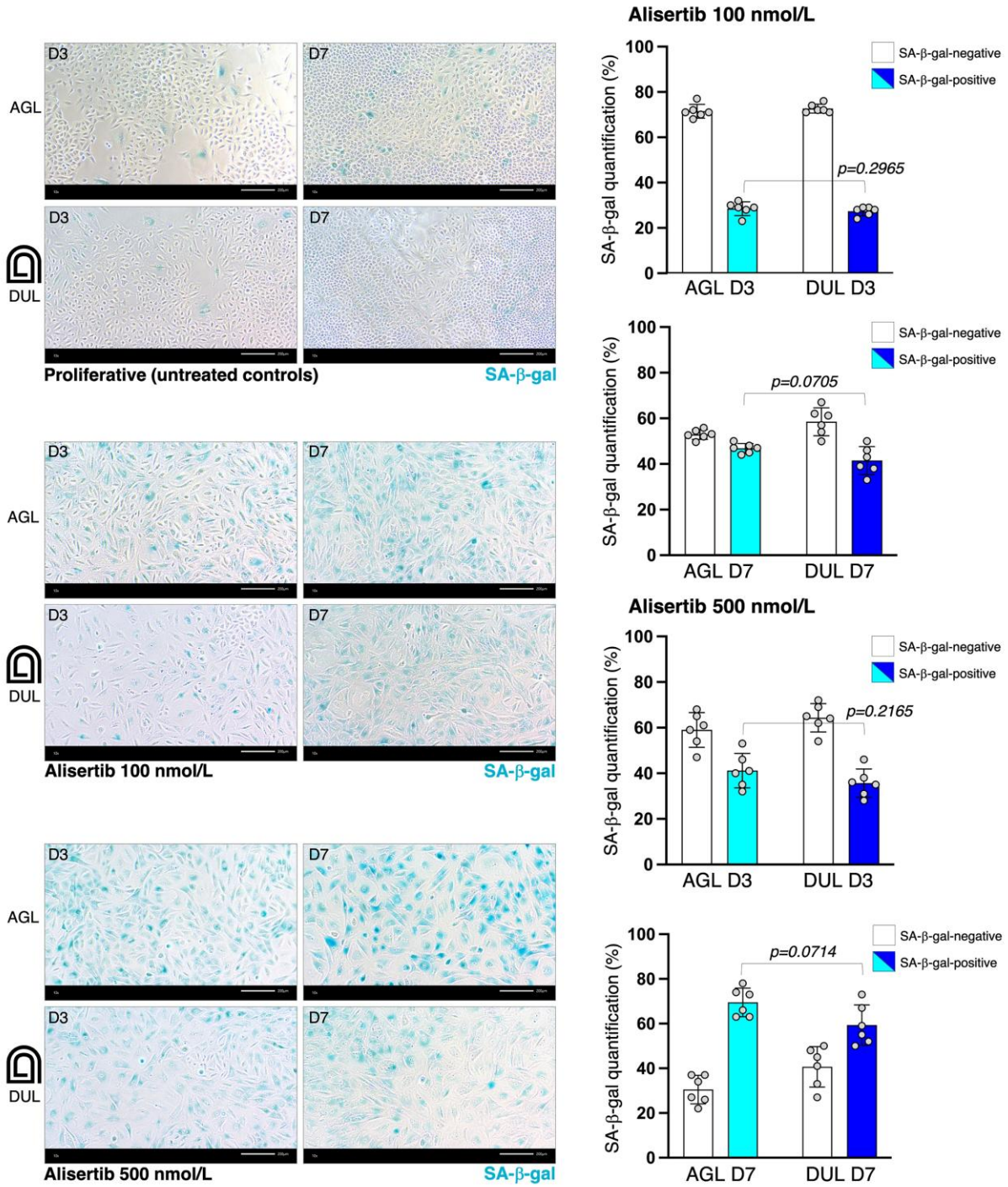

Figure 5. Cosmic silence does not significantly modify the induction kinetics of alisertib-triggered SA-β-gal-positive senescent states. This figure provides a quantitative assessment of senescence-associated β-galactosidase (SA-β-gal) activity in A549 cells exposed to low- and high-dose alisertib (100 and 500 nmol/L) under standard (above-ground laboratory, AGL) and muon-depleted (deep-underground, DUL) radiobiological conditions. The cells were pre-acclimated for nine days to their respective environments before treatment and analyzed at the early (day 3, D3) and late (day 7, D7) stages of therapy-induced senescence. *Left panels.* Representative microphotographs illustrate the extent of SA-β-gal-positivity commonly associated with lysosomal expansion occurring in senescent cells. Scale bars, 200 µm. *Right panels.* The quantification of at least 2,000 cells per condition is shown as a percentage of SA-β-gal-negative (white) and SA-β-gal-positive (blue) cells. Data represent the mean ± S.D. (n=2 independent biological replicates; n≥3 technical replicates for each condition). *p* values shown were calculated using a two-sided non-parametric Mann–Whitney U test and are presented for exploratory comparison.

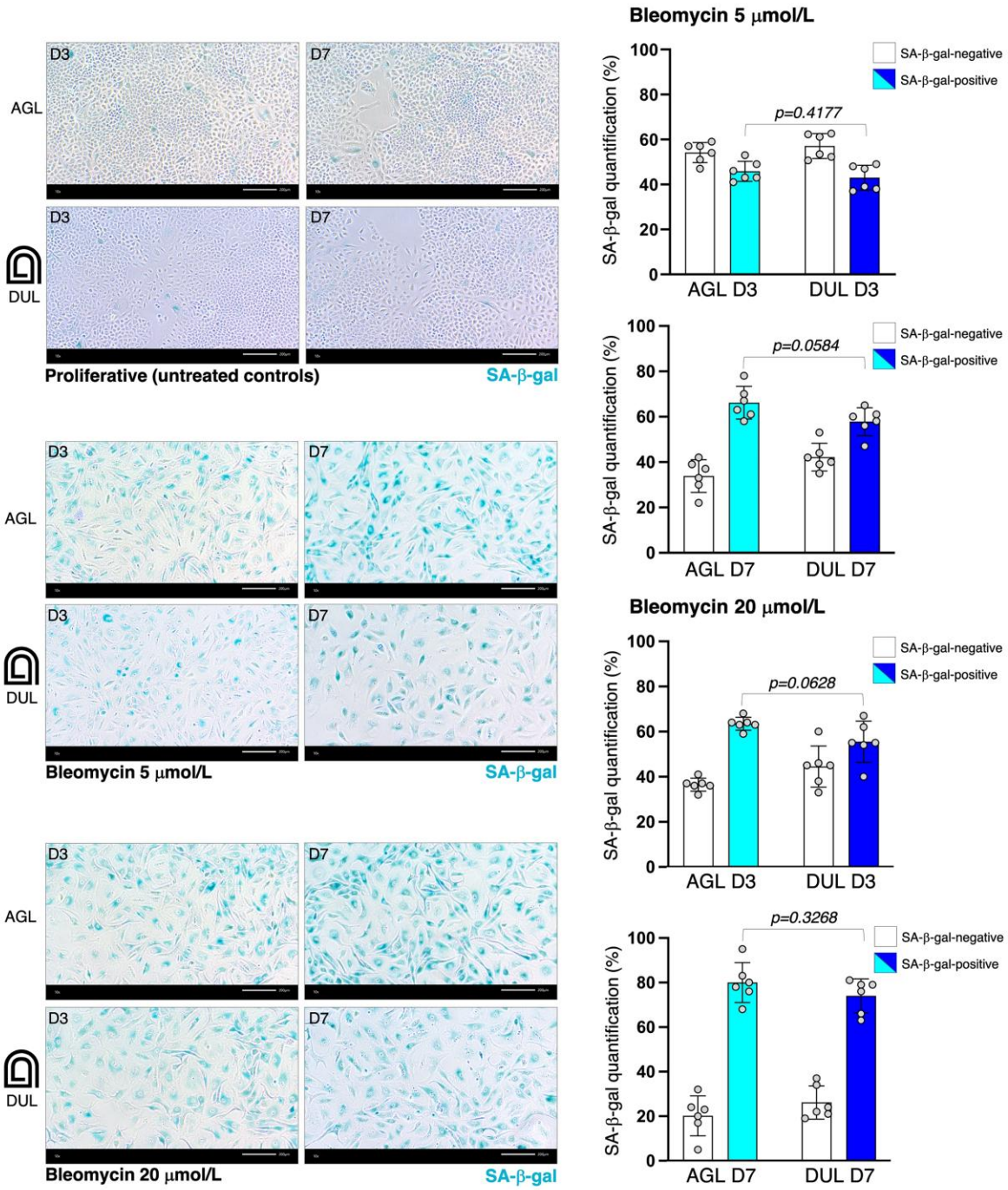

Figure 6. Cosmic silence does not significantly modify the induction kinetics of bleomycin-triggered SA-β-gal-positive senescent states. This figure provides a quantitative assessment of senescence-associated β-galactosidase (SA-β-gal) activity in A549 cells exposed to low- and high-dose bleomycin (Aurora A kinase inhibitor; 5 and 20 μmol/L) under standard (above-ground laboratory, AGL) and muon-depleted (deep-underground, DUL) radiobiological conditions. The cells were pre-acclimated for nine days to their respective environments before treatment and analyzed at the early (day 3, D3) and late (day 7, D7) stages of therapy-induced senescence. *Left panels.* Representative microphotographs illustrate the extent of SA-β-gal-positivity commonly associated with lysosomal expansion occurring in senescent cells. Scale bars, 200 μm. *Right panels.* The quantification of at least 2,000 cells per condition is shown as a percentage of SA-β-gal-negative (white) and SA-β-gal-positive (blue) cells. Data represent the mean ± S.D. (n=2 independent biological replicates; n≥3 technical replicates for each condition). *p* values shown were calculated using a two-sided non-parametric Mann–Whitney U test and are presented for exploratory comparison.

Cosmic silence does not significantly reduce the number of SA-β-gal-positive senescent cells induced by alisertib and bleomycin

A completely different picture emerged when the G0/G1-targeting stressor palbociclib was replaced with the G2/M-targeting stressor alisertib. Both low (100 nmol/L) and high (500 nmol/L) concentrations of alisertib produced a similar increase in the number of SA-β-gal-positive cells during the early stages of senescence regardless of the AGL/DUL environment (Fig. 5). There was slightly lower but not statistically significant SA-β-gal positivity at the late stage of alisertib-induced senescence in the DUL environment regardless of the alisertib dose (Fig. 5).

A low concentration of the G2/M-targeting stressor bleomycin (5 µmol/L) produced a similar increase in the number of SA-β-gal-positive cells at the early stage of senescence. There was also a non-statistically significant trend toward lower SA-β-gal positivity at the late stage in the DUL environment (Fig. 6). A high concentration of bleomycin (20 µmol/L) produced a similar percentage of SA-β-gal positive cells regardless of stage (early or late) or AGL/DUL environment (Fig. 6).

SA-β-gal-positivity was slightly but significantly lower for the G0/G1-targeting stressor palbociclib and remained largely unaltered for the G2/M-targeting stressors alisertib and bleomycin under the muon-depleted radiobiological conditions of the DUL. These findings can be summarized by a hypothetical model that accounts for the integrated stress signaling, i.e., the sum of drug-driven damage load and the "muon calibration" required to reach and cross the threshold for acquiring the SA-β-gal-positive senescent phenotype (Fig. 7). Under muon-depleted DUL conditions, those cells that become SA-β-gal-positive after G0/G1-directed stress are selectively affected by the loss of muon calibration. In contrast, the higher damage load of those cells undergoing G2/M-like arrest to become senescent in response to alisertib or bleomycin largely overrides the muon-dependent calibration, achieving the SA-β-gal positive state with or without cosmogenic muons (Fig. 7).

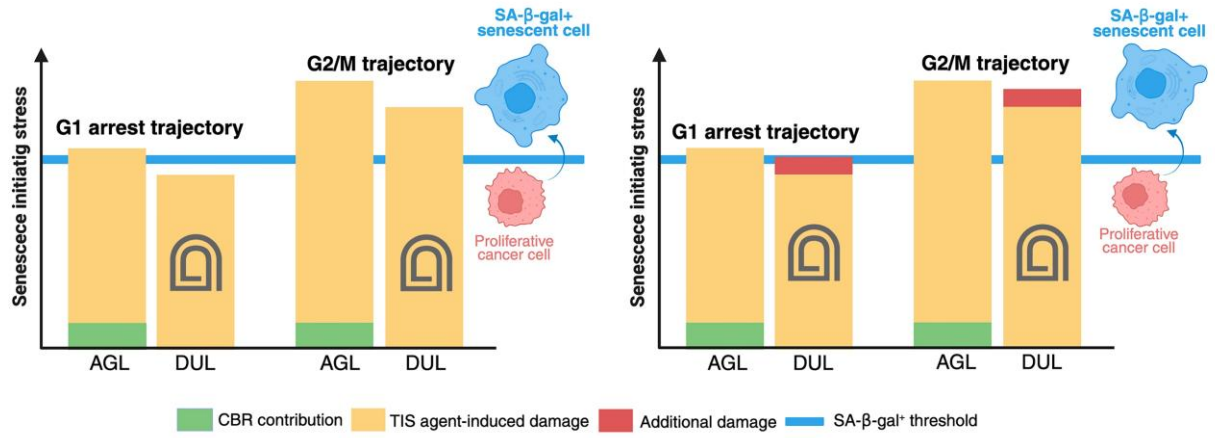

Figure 7. Ambient muons and the entry threshold to SA-β-gal-positive senescent states: A hypothetical calibration model. This stacked bar model summarizes the findings from Figures 3, 4 and 5 regarding G0/G1-targeting palbociclib and G2/M-targeting alisertib and bleomycin senescence stressors in AGL (surface) versus DUL (cosmic silence) environments. The blue threshold line indicates the minimum stress signal needed to reach an SA-β-gal$^+$ senescent state. The green bars quantify the abiotic CBR ("muon") contribution present at AGL and absent at DUL. The yellow bars represent the drug-evoked stress/damage load, and the red bars indicate any additional stress/damage that could accrue in the DUL. Eliminating muons therefore removes a component of the cumulative damage budget (i.e., damage signaling and/or self-reinforcing loops. The hypothetical, parsimonious scenario on the *left* considers that although cells do not accumulate more damage in the DUL than in the AGL, muon depletion can prevent cells from reaching the threshold for acquiring an SA-β-gal$^+$ senescent phenotype. The hypothetical permissive scenario on the *right* considers that, although cells accumulate more damage in the DUL than in the AGL, muon depletion can still prevent cells from transducing sufficient signaling amplitude to cross the threshold for SA-β-gal-positivity. When the integrated damage signal falls below the threshold, acquisition of an SA-β-gal$^+$ phenotype is prevented. In both scenarios, this explains the quantitative loss of SA-β-gal$^+$ cells in response to G0/G1-targeting stressors such as palbociclib, but not in response to the G2/M-targeting stressors, such as alisertib and bleomycin. Together, the schematics formalize ambient muons as an abiotic rheostat that tunes commitment to a late, hard-locked senescent (SA-β-gal-positive) state, which is most evident under G0/G1-driven senescent trajectories. However, G2/M-driven senescent trajectories largely override the radiobiological threshold for establishing SA-β-gal$^+$ cellular states and proceed robustly despite muon depletion.

Cosmic silence does not alter the qualitative transcriptomic senescence scores of senescent-inducing agents

Next, we aimed to assess whether cosmic silence's ability to reduce the number of SA-β-gal-positive cells in response to palbociclib, but not to alisertib and bleomycin, was related to changes in the execution of a well-established transcriptional signature of senescence.

We applied SENCAN, a machine learning–based senescence predictor that calculates the likelihood of senescence (between 0 and 1) using only RNA-seq data, to the results obtained. This 137-gene, elastic-net-based classifier was constructed using bulk RNA sequencing data from 13 cancer cell lines that were induced to senesce via alisertib and etoposide treatment [89]. Thus, SENCAN is particularly robust at detecting the senescent state in cancer cell populations compared to other conventional senescence hallmark gene signatures developed from normal cells [89].

Analyzing the RNA-seq data with the SENCAN classifier revealed that under AGL control conditions, a low dose of palbociclib (1 μmol/L) yielded lower transcriptional scores in the early (~0.5) and late (~0.7) stages compared to a higher dose of palbociclib (5 μmol/L), which produced SENCAN scores ≥0.9 regardless of stage (Fig. 8). These results confirmed the previously reported weaker strength and shallower senescence deepening induced by palbociclib. The transient senescence-associated maintenance mechanisms triggered by palbociclib allow cells to reenter the cell cycle and regain proliferative capacity when the drug is not continuously provided [101,116–119]. This contrasts with the more stable, full-blown arrest states triggered by alisertib and bleomycin. Accordingly, the SENCAN transcriptional scores of the bleomycin and alisertib TIS populations were consistently high (≥0.9) regardless of dosage or the timepoint of senescence (Fig. 8).

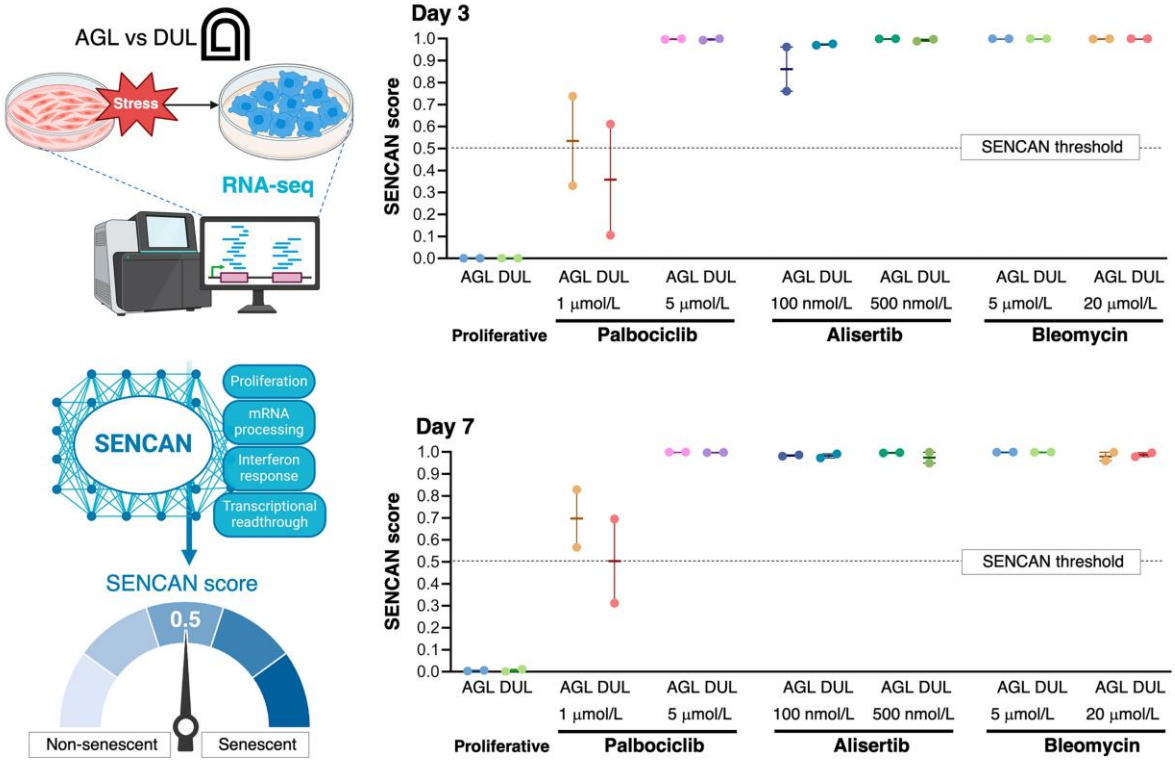

Figure 8. Cosmic silence largely preserves the senescence-like transcriptomic identity of TIS phenotypes. *Left.* We applied the SENCAN classifier tool to RNA-seq data obtained from untreated proliferative controls and chemotherapy-treated cell populations under AGL and DUL radiobiological environments. SENCAN is based on 137 genes, including known "standard" senescence-associated genes (e.g., *CDKN1A* and *HMGB1*) as well as genes involved in mRNA processing and splicing (e.g., *SNRPA* and *SRSF2*), interferon response genes (*IFIT2* and *ISG15*), and signals derived from transcriptional readthrough *(*e.g., AL512306.2, downstream of MDM4) [89]. This makes SENCAN particularly robust for detecting the senescent state in cancer cells compared to other conventional senescence hallmark gene signatures developed from normal cells. *Right.* Figure shows the RNA-seq-derived probability of the presence of a senescence transcriptomic signature (SENCAN; 0–1) in A549 cells after treatment with palbociclib (1 and 5 μmol/L), alisertib (100 and 500 nmol/L) or bleomycin (5 and 20 μmol/L) in AGL versus DUL "cosmic silence" for three (*top*) and seven (*bottom*) days. The graph shows the 95% confidence intervals for the mean SENCAN scores obtained from RNA-seq data of 2 independent biological replicates.

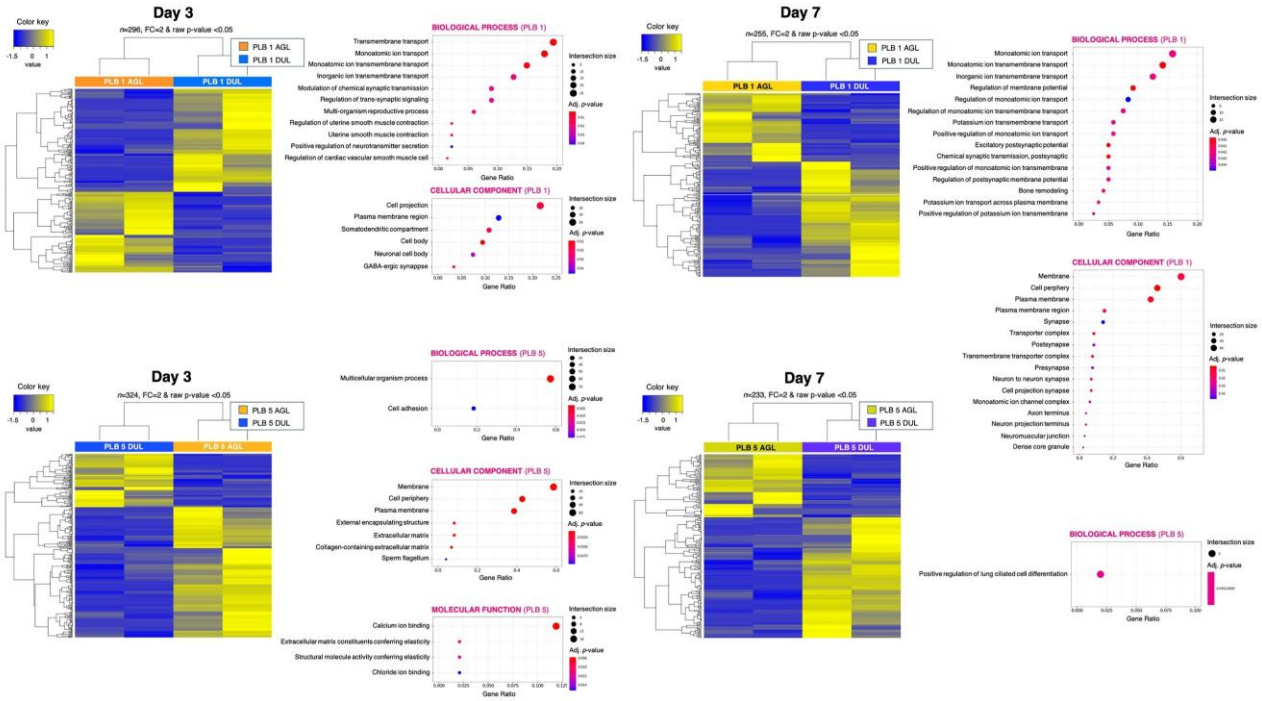

Figure 9. Differential transcriptomic responses to palbociclib in AGL and DUL environments. Figure shows two-way, unsupervised, hierarchical heatmaps of DEGs identified in each contrast (rows, genes; columns, samples). The values are z-scores per gene computed from log2-based expression values. Only genes with a |fold-change| ≥2 and a raw p<0.05 were included (n=2 independent biological replicates). The four gene sets comprise PLB 1 µmol/L day 3 (n=296), PLB 5 µmol/L day 3 (n=324), PLB 1 µmol/L day 7 (n=255), and PLB 5 µmol/L day 7 (n=233), comparing AGL vs. DUL conditions. The sample labels above each heatmap indicate the treatment (PLB 1 or 5 µmol/L), the time point (day 3 or 7), and the environment (AGL or DUL). Color keys denote relative expression (low to high) after z-score normalization. Gene Ontology (GO) enrichment analyses were performed on the DEG sets and are summarized by the three GO domains: Biological Process, Cellular Component, and Molecular Function. For each contrast, the most significantly enriched terms within each domain are displayed and ranked by significance within the category.

Slightly decreased SENCAN scores were observed during the early (3 days) and late (7 days) stages of the TIS phenotype triggered by a low dose (1 µmol/L) of palbociclib in the muon-less cosmic silence within the DUL environment. These samples received non-senescent scores of 0.1 and 0.3 on days three and seven, respectively, in one of the biological replicates. The SENCAN score can only classify a sample as senescent if the majority of cells are senescent [89], thus suggesting that the muon-less DUL environment reduces the number of senescent cells in the palbociclib-treated cell populations. However, the overall decrease was not statistically significant. Furthermore, these differences were no longer evident when a higher dose of palbociclib (5 µmol/L) was used (Fig. 8). The SENCAN transcriptional scores of the bleomycin and alisertib TIS were extremely high and indistinguishable under AGL and DUL conditions, regardless of dosage or the timepoint of senescence (Fig. 8).

Together, these data show that cosmic silence does not qualitatively reprogram the senescence-induced transcriptome state caused by G2/M-directed stressors (alisertib and bleomycin) and exerts, at most, a modest effect on the response to low doses of the G0/G1-directed stressor (palbociclib). Therefore, reduced SA-β-gal positivity under DUL conditions does not correspond to a collapse of canonical senescence transcriptional signatures. This finding supports the idea that the effect of cosmic silence on senescent-cell abundance is primarily quantitative rather than a qualitative shift in senescence identity.

Cosmic silence alters the coding transcriptome of palbociclib-induced senescent states

Transcriptome signatures can be associated with specific senescence-inducing stresses, and different senescent trajectories can drive a variety of senotypes depending on cell-cycle arrest pathways [120–126]. Thus, we examined the impact of muon absence on the entire transcriptional landscape of the senescence program triggered by palbociclib, beyond the SENCAN score.

First, we examined the response of the coding transcriptome to graded concentrations of palbociclib in AGL and DUL environments using volcano plots (Supplementary Fig. 1). Within each environment,

palbociclib versus proliferative controls yielded robust, time- and dose-dependent distributions of differentially expressed genes (DEGs), with broad log_2 fold change (log2 FC) dispersion and an elevated false discovery rate (FDR). Overlaying the AGL and DUL volcano plots at a matched dose and time revealed that the distributions generally coincided in terms of effect size and significance. This cancels out most of the baseline differences observed when comparing palbociclib-treated cells to their respective site's proliferative (untreated) controls. Minor local asymmetries, particularly at 1 µmol/L palbociclib, were visually modest and did not disrupt the overall overlap. These results suggest that environment-specific contrasts apparently disappear when considering palbociclib exposure and duration.

The overlap of volcano plots only determines if the exact same individual genes pass an arbitrary *p*-value value/|log_2FC| cutoff in both conditions. Comparing the two binary DEGs lists (AGL vs. DUL) is not very powerful and is sensitive to list length, which is influenced by small shifts around the FDR or log2FC cutoffs. Therefore, we investigated whether the radiobiological environment rather affected coordinated patterns across many genes relative to the expressed background rather than individual genes. This approach is more powerful when many genes change modestly yet coherently, resulting in an aggregate signal that survives the DEG volcano plots thresholding idiosyncrasies. We performed an unsupervised hierarchical clustering analysis of DEGs and classified them into enriched categories of biological processes (BP), cellular components (CC), and molecular functions (MF) using Gene Ontology (GO) analysis (Fig. 9). At the early stage of senescence (3 days), the top BP clustered categories that distinguished palbociclib TIS under AGL and DUL conditions were enriched in genes involved in transmembrane ion transport and multicellular organismal processes. The CC categories that were more significantly enriched and distinctive of palbociclib TIS under AGL and DUL conditions were cell projection and plasma membrane. The MF category with the highest enrichment discriminating palbociclib TIS under AGL and DUL conditions was calcium ion binding. At the late stage of senescence (7 days), the BP categories that were more significantly enriched and distinctive of palbociclib TIS under AGL and DUL conditions were monoatomic/inorganic ion transport and positive regulation of lung ciliated cell differentiation. The CC categories with the highest enrichment discriminating palbociclib TIS under AGL and DUL conditions were the cell plasma membrane, transmembrane transport, and cell projections.

Finally, we used Venn diagrams to identify transcriptomic features that were uniquely regulated by the palbociclib TIS phenotype, as compared to the untreated proliferative counterparts, in the AGL and DUL environments (Supplementary Fig. 2). Notably, the number of DEGs that were exclusively and significantly up- or down-regulated in the cosmic silence of the DUL environment was consistently lower than in the AGL control environment. We performed a functional enrichment analysis of the exclusive DEGs that did not overlap between the AGL and DUL conditions using the EnrichR database. Early in the senescence process (3 days), terms related to the p53 pathway and epithelial-to-mesenchymal transition (EMT) were significantly enriched in the palbociclib TIS phenotype occurring in cosmic silence. The enrichment scores were low but statistically significant. At the late stages of senescence (7 days), the GO terms most significantly depleted in the palbociclib TIS phenotype occurring in cosmic silence were related to the G_2-M checkpoint and E2F target genes.

DUL conditions without muons do not appear to drastically alter the core transcriptional program of the senescent state induced by palbociclib. Rather, they appear to subtly adjust the expression of genes whose products are involved in organizing cell membranes and ion flux in palbociclib-treated cells. This includes binding of Ca^{2+}, transmembrane transport, and factors involved in cell projection and ciliogenesis. These differences are mechanistically compatible with senescence biology, including remodeling of the cell surface, altered membrane potential, and Ca^{2+} and broader ion homeostasis modules [127–134]. They likely represent environmental fine-tuning of the communication interface rather than a significant departure from the canonical senescence identity. Indeed, the occurrence of fewer exclusive DEGs inside the DUL suggests a more compressed palbociclib-senescence program under muon depletion. Early DUL-exclusive enrichments are consistent with the transient activation of stress/epithelial-plasticity circuits that can prepare cells for eventual TIS escape if arrest fluctuates or erodes [135–137].

The coding transcriptome of bleomycin-induced senescent states is largely unresponsive to cosmic silence

We then explored whether the coding transcriptomes of senescent states driven by a G2/M arrest trajectory (alisertib and bleomycin) were impacted as much as those of senescent states driven by a G0/G1 arrest trajectory (palbociclib).

We first used Venn diagrams to determine the number of transcriptomic features that were uniquely regulated by the TIS phenotypes generated by G2/M-targeting stressors in the AGL and DUL environments (Supplementary Fig. 3). As in the case of palbociclib, the number of DEGs that were exclusively and significantly

up- or down-regulated in the cosmic silence of the DUL environment was consistently lower than in the AGL control environment in response to low- and high-concentrations of alisertib. While such a trend was apparent when using the lowest concentration of bleomycin early in the senescence process (3 days), no differences were observed in response to the highest of concentration of bleomycin.

We then performed an unsupervised hierarchical clustering analysis of DEGs and classified them into enriched categories of BP, CC, and MF using GO analysis (Supplementary Fig. 4,5). At the early stage of alisertib-induced senescence (day 3), the transcriptomic differences between AGL and DUL were primarily associated with multicellular and developmental programs, cell adhesion, ciliogenesis and cell motility, and cell-surface receptor signaling. There was also enrichment of cell periphery, plasma membrane, and cell projection CC terms, as well as receptor-regulatory, cytokine, and growth factor MF categories, particularly at the highest alisertib concentration. (500 nmol/L). By day 7, a clear shift emerged at the 100 nmol/L alisertib stage, with the appearance of glucuronidation-related BP and MF categories, including cellular glucuronidation, glucuronate/uronic acid metabolic processes, and the regulation of glucuronosyltransferase activity (Supplementary Fig. 4). Together with these, membrane/cell periphery/plasma membrane and passive transmembrane transport/channel activity terms appeared. In contrast, the 500 nmol/L alisertib condition was still dominated by broader multicellular organismal and membrane-, extracellular-, and cell-projection-related categories. The late enrichment in glucuronidation-linked functions is noteworthy because alisertib undergoes both oxidative metabolism and direct acyl-glucuronidation. The uridine 5′-diphospho-glucuronosyltransferase 1A1, 1A3, and especially 1A8 enzymes contribute to this pathway [138]. This may indicate a distinct adaptive metabolic detoxification response to prolonged alisertib exposure in AGL vs DUL radiobiological environments, rather than a change in the senescence program itself.

In contrast to alisertib, bleomycin-induced senescence showed an almost complete absence of robust GO enrichments, despite transcriptional differences between AGL and DUL conditions (Supplementary Fig. 5). Only a few isolated terms emerged –mainly extracellular region, cell periphery and plasma membrane, and outward rectifier potassium channel activity, arguing against a coherent environment-specific functional rewiring. Mechanistically, this suggests that bleomycin drivers a more convergent, damage-dominated senescent state, with little evidence for the layered adaptive programs seen with alisertib.

Across G0/G1 and G2/M-related senescence trajectories, cosmic silence appears to shape the coding transcriptome along a graded continuum rather than through a uniform effect. Palbociclib exhibits subtle yet noteworthy remodeling, primarily in membrane, ion transport, and cell projection programs. Alisertib adds a robust late adaptive component associated with glucuronidation-related drug detoxification, while bleomycin exhibits minimal coherent functional rewiring. These results suggest that the impact of the muon-depleted DUL radiobiological environment depends on the senescence trajectory and the nature of the inducing stress. This impact is more evident when cells retain programs associated with proliferation (palbociclib) or adaptive pharmacologic responsiveness (alisertib) than when they are in a predominantly damage-dominated state (bleomycin).

Cosmic silence does not significantly alter the composition of TIS-associated SASPs

We then assessed whether the composition of TIS-associated secretomes varied in response to the muon-less environment of cosmic silence in the LSC-DUL. Cell culture supernatants were collected simultaneously from non-senescent (proliferative control) cells and from A549 cells that were made senescent with palbociclib, alisertib, and bleomycin at the AGL and DUL facilities. We analyzed the samples using a panel of 96 cytokine, chemokine, and growth factor biomarkers with a multiplex bead-based Luminex® immunoassays. We generated heatmaps of secretomes according to the AGL/DUL localization, time of exposure, and TIS inducer concentration, using $\log_2$ transformed values (Fig. 10). We $\log_2$ transformed all the concentration values because the raw values were strongly skewed, ranging from ~1 pg/mL to > 10,000 pg/mL for a single analyte within a given dataset. As previously recommended, log transformation makes the distribution of values much easier to work with, reduces the likelihood of erroneously excluding large values as outliers, and generally makes outlier detection easier [139,140].

First, and in agreement with previous studies, all the TIS stressors generated SASP landscapes that were largely dictated by the baseline secretome of the cell-of-origin (A549) [89,112]. Second, a slightly higher expression of SASP components was apparent in G2/M stressors, particularly alisertib, in comparison to palbociclib. Radiobiological conditions did not appear to significantly alter the baseline composition of the secretome in A549 proliferative cells grown for 3, 5, and 7 days in AGL and DUL facilities (Fig. 10A). The qualitative composition of each SASP and the quantitative expression of specific SASP components did not exhibit

highly significant changes when comparing AGL and DUL environments. Palbociclib elicited an early, compositionally focused SASP that accumulated similarly in AGL and DUL environments. However, conversion to broader late SASP modules was modestly attenuated in the muon-depleted DUL environment (Fig. 10B). With alisertib and bleomycin, however, we observed a high-amplitude, environment-insensitive SASP landscapes (Fig. 10C).

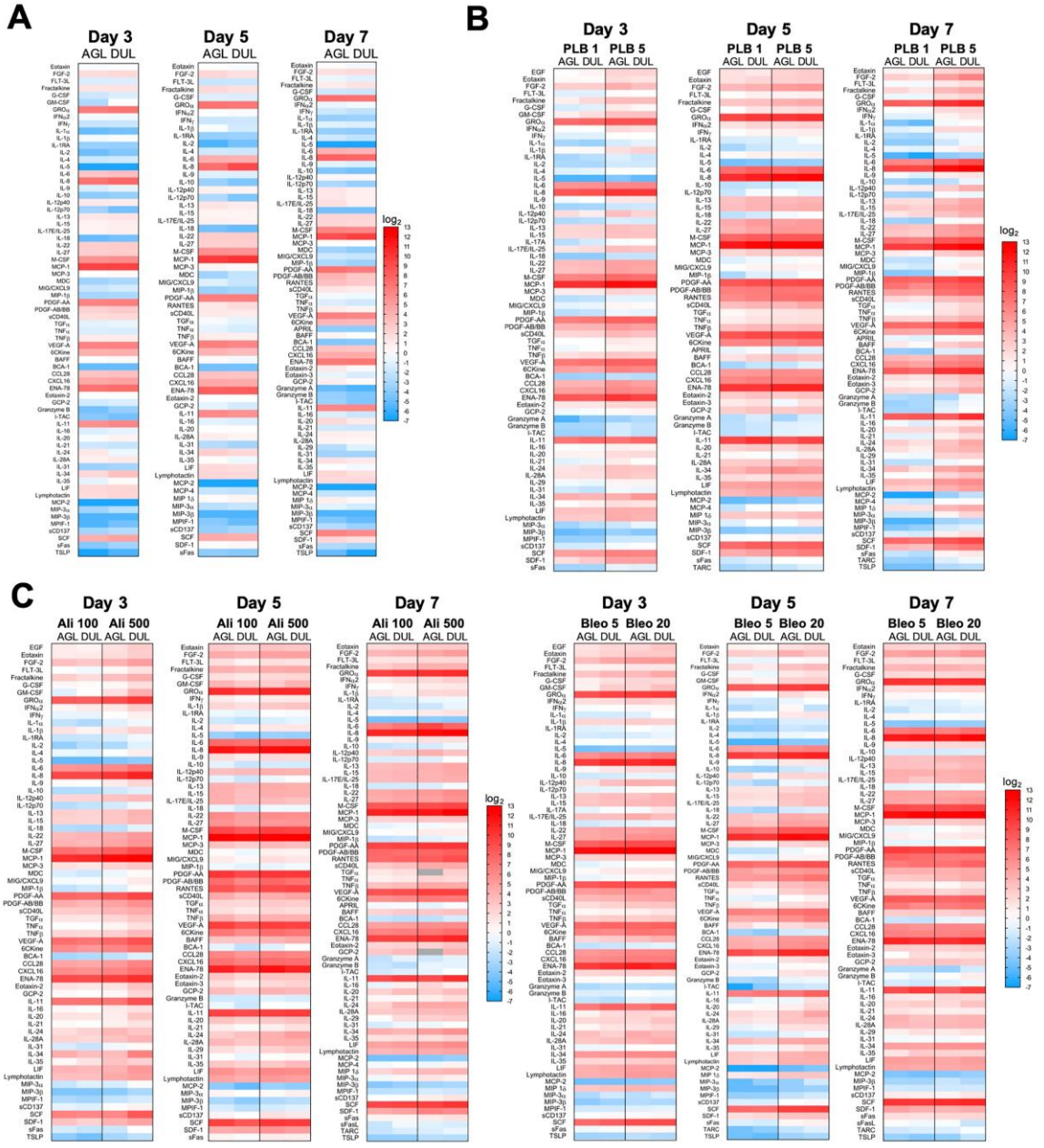

Figure 10. Cosmic silence largely preserves SASPs across TIS phenotypes. The qualitative and quantitative composition of the extracellular secretome in cell-free supernatants collected under above-ground (AGL) and deep-underground (DUL) conditions across proliferative and specified pharmacological perturbations was characterized using multiplex bead-based immunoassays on days 3, 5 and 7. For all heatmaps, each cell represents the measured concentration for a single analyte (row) in the indicated condition (column). Color scale encodes $\log_2$-transformed raw abundances ($\log_2$ scale of the unnormalized measurements; n=2 independent biological replicates), enabling comparison of composition (relative factor weighting) across conditions while stabilizing variance and dynamic range. Columns are organized by environment (AGL, DUL) and time; drug panels additionally stratify by dose. These visualizations allow direct comparison of environment-dependent basal secretion and treatment-dependent remodeling at matched time points and doses.

Taken together with the fact that SENCAN scores remained unchanged, the data suggest that muon depletion in the DUL environment does not significantly interfere with the initiation of early programming of senescence following chemotherapy. This is evident because transcriptional senescence modules, as well as the qualitative composition and quantitative levels of the diverse SASPs, activate normally and remain globally similar between the AGL and DUL environments. The lower background radiogenic stress in the DUL environment slightly shifts the SA-β-gal+ threshold in response to palbociclib. This can explain the reduced effectiveness of the paracrine amplification and the phenotypic consolidation of SA-β-gal+ phenotypes, as expected from the feed-forward bystander signaling of the SASP (e.g., secondary senescence). In contrast, alisertib and bleomycin generate sufficient intrinsic damage signaling to overcome this dependency. This results in an environment-invariant SASP and late SA-β-gal+ senescence. These findings support the notion that cosmic silence could limit the propagation of TIS phenomena following low-intensity, G0/G1-arrest-like trajectories (palbociclib) while remaining largely irrelevant in cases of high-intensity G2/M arrest.

DISCUSSION

Our study provides the first formal but exploratory evidence that CBR might be mechanistically incorporated into the operability of cellular senescence programs in human cells. Our study suggests that muon depletion does not uniformly suppress the occurrence of senescence following chemotherapy-induced cellular damage. Rather, it might preferentially affect the consolidation of specific senotypes. In the ultra-low CBR environment of the LSC-DUL, the most consistent finding was a slightly reduced ability of the G0/G1 arrest stressor palbociclib to generate robust SA-β-gal-positive states, especially at low concentrations. Meanwhile, SA-β-gal-positive states arising from G2/M arrest stressors, such as the mitotic kinase inhibitor alisertib and the radiomimetic bleomycin, remained comparatively stable. Highly conserved transcriptomic senescence scores (i.e., SENCAN) and the SASP remained largely intact, regardless of the senescence-induction trajectory. Taken together, these hypothesis-generating observations argue against a global failure of senescence induction in the absence of cosmic ray muons. Instead, they suggest a more selective impact of cosmic silence on the progression from early senescence-associated programs to well-established SA-β-gal-positive senescent states when involving G0/G1 (but not G2/M) cell cycle withdrawal trajectories. These findings could help us understand how the radiobiological calibration of senescence programs has evolved to ensure commitment to terminal senescence under weak, yet physiologically relevant stresses (e.g., replicative senescence), while allowing severely damaged cells to transition immediately to hard-locked senescence, regardless of the CBR context.

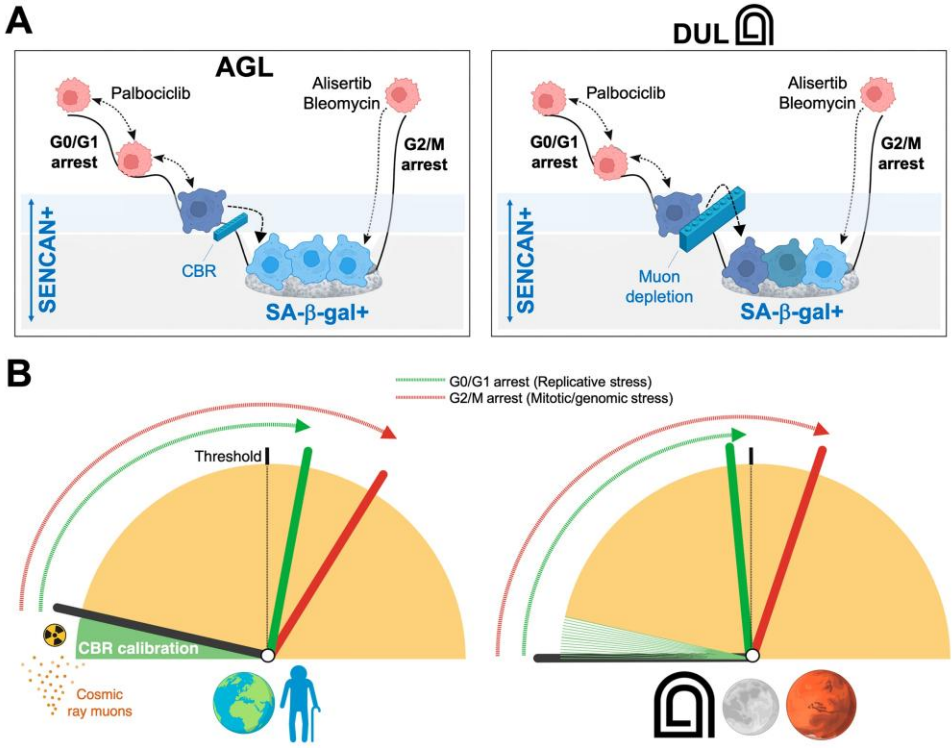

Figure 11. A model of cosmic background radiation-regulated therapy-induced senescence. A. An energy landscape based on the Waddingtonian model and incorporating the aforementioned findings can illustrate how senescence-related SA-β-gal+ status and transcriptomic readouts can be theoretically reconciled. In the palbociclib-targeted G0/G1-like arrest trajectory, muon depletion minimally alters the rapid entry into the shallow, SENCAN+ transcriptome basin, but significantly reduces the flux into the ultimate SA-β-gal+ basin. Under DUL conditions, the loss of stochastic CBR "kicks" could lower the barriers to cell-cycle re-entry, thereby reducing progression towards deeper arrest intensity. This could result in cells remaining SENCAN+ but failing to hard-lock into the deepest, converging level of SA-β-gal+ attractors. Conversely, those cells following a G2/M arrest trajectory (e.g., alisertib and bleomycin) can transition directly to an SA-β-gal-positive state, regardless of the muonic environment. Across contexts, early transcriptional priming (elastic-net SENCAN classifier) occurs similarly before SA-β-gal-positive states are reached, regardless of the path to arrest. However, the probability of reaching the SA-β-gal-positive state without completing the proliferation-quiescence-senescence continuum is CBR-sensitive only when cells follow the G0/G1-arrest path. Nevertheless, although muon depletion does not appear to drastically alter the genes and processes that are universally changed in senescent cells (e.g., those captured by the SENCAN score), the degree of overlap between the AGL and DUL senotype transcriptomes varies depending on the stressor. This divergence is more apparent in the G0/G1 senescence trajectory triggered by palbociclib and is almost non-existent in the G2/M trajectory triggered by bleomycin. **(B)** Ambient cosmogenic muons at the Earth's surface introduce a stochastic damage and damage-reinforcing signaling loops that calibrate the threshold for committing proliferative cells to the late, lysosome-dependent, SA-β-gal+ senescent state. In muon-depleted settings (deep underground or on the Moon or Mars), this term is absent, and low-DDR inputs fall below the commitment barrier, decreasing the effective crossing rate. The length of the arrow encodes DDR amplitude (green for low and red for high) relative to the SA-β-gal threshold. The "CBR calibration" needle denotes the muon contribution present at the surface and lost underground. Consequently, muons act as an abiotic rheostat that selectively enables barrier crossing under weak replicative stress (e.g., palbociclib or olaparib in HR-proficient cells), whereas strong genotoxic stress (e.g., alisertib, bleomycin or olaparib in HR-deficient cells) surpasses the threshold irrespective of the muon background.

The differential effect of cosmic silence can be preliminarily interpreted as the modulation of commitment along specific senescence trajectories (Fig. 11A). The G0/G1 arrest pathway, which is preferentially engaged by palbociclib and remains closer to the quiescence-senescence boundary [126,141,142], may depend more on weak background inputs, such as stochastic muonic "kicks", to gradually progress into deeper SA-β-gal-positive senescent states. In contrast, the G2/M arrest trajectory, engaged by alisertib and bleomycin, rapidly and forcefully propels cells toward an insurmountable, stable arrest. This trajectory is highly refractory to muon depletion. Thus, the key effect of muon depletion may not be the entry into a senescence-like program *per se*, but rather the reduction of the probability that cells traversing a gradual G0/G1 withdrawal route will fully consolidate into an SA-β-gal-positive senotype. Background muons may therefore act as weak abiotic contributors to the signal-to-noise architecture of senescence commitment. Under above-ground conditions, chronic environmental radiation may provide a small but persistent source of background damage or checkpoint priming that facilitates the transition into deeper senescent states when the primary arrest stimulus is modest. Underground, removing the muonic background input would be expected to most impact trajectories that rely on gradual proliferative withdrawal (the G0/G1 path). This would have a much smaller or null effect on trajectories that are strongly driven into post-replicative or mitotic arrest by the senescence-inducing stressor (the G2/M path).

This framework also explains the apparent discrepancy between preserved transcriptome senescence scoring and reduced SA-β-gal-positivity in response to palbociclib. If early senescence-associated remodeling in the G0/G1 arrest pathway progressively emerges with a declining probability of cell-cycle reentry, then palbociclib-treated cells may still enter a senescence-leaning transcriptional state while failing to undergo the lysosomal and phenotypic remodeling associated with robust SA-β-gal positivity. The selective sensitivity of low-dose palbociclib to cosmic silence is therefore consistent with an impairment in senotype consolidation rather than a complete loss of senescence-associated transcriptional reprogramming. Muon depletion does not significantly alter the fundamental transcriptional architecture of senescence, such as the gene programs captured by the SENCAN score. However, it modulates the degree to which AGL and DUL senotypes converge at the transcriptional level, depending on the stress pathway that induces them. This stress dependence suggests that the radiobiological environment impacts the transcriptional signatures of AGL/DUL senotypes initiated through a G0/G1 arrest trajectory more than it impacts the more convergent, G2/M arrest-driven transcriptional signatures of AGL/DUL senotypes induced by alisertib and bleomycin. The SASP behaves in a manner that follows the same hierarchy as the senescence-related transcriptional signatures. The qualitative composition of the diverse SASPs is broadly conserved between AGL and DUL. Palbociclib elicits an early, focused SASP in both environments, with slightly

blunted broadening at a later time in DUL. Conversely, G2/M arrest-related SASPs, on the other hand, are high-amplitude and environment-insensitive. Thus, the early senescence transcriptomic program, including the expression of qualitative SASP components initiates normally without muons. However, the competence of neighboring cells to adequately interpret the stress communication via the SASP diminishes in the absence of baseline radiation-primed responsiveness. Therefore, the SASP produced under these muon-depleted conditions is insufficient for a paracrine propagation of senescence, even when it is quantitatively and qualitatively indistinguishable from that activated at the surface. This could explain why the expected paracrine/bystander effect of senescence reinforcement via the SASP, which normally helps consolidate SA-β-gal-positive states under weak stress, is significantly less effective underground.

Although our data are consistent with a model in which cosmic silence fine-tunes stress-specific senescence outputs rather than the core senescence backbone, one might argue that the present study did not identify the precise senescence traits mediating this effect. Nevertheless, the reduced arrest intensity we observed is unlikely to result from a single switch-like transcriptional change. Rather, it likely reflects variation across multiple senescent traits. Consistent with this idea, none of the small but significantly enriched GO terms distinguishing palbociclib-driven TIS in AGL vs DUL environments mapped directly to well-established senescence transcriptomic signatures. However, the enrichment of quiescent/ciliated differentiation, which promotes a cell-cycle exit overlapping with senescence, and altered ion homeostasis, which could reflect a reduced lysosomal mass and acidification while increasing lysosomal exocytosis, suggests that the absence of CBR shifts some cell subpopulations toward a less consolidated senescence-like arrested state [127–134,143–145]. EMT, which promotes early palbociclib resistance and prevents palbociclib-driven long-term E2F-controlled cell-cycle arrest and senescence [119], was also enriched in the DUL environment. Thus, muon depletion may alter the multistep response to palbociclib by shifting the balance from maintenance of arrest toward resistance development, ultimately impairing lysosomal remodeling and favoring long-term escape from senescence [119,136,137]. An alternative explanation is that the DUL environment selectively dampens the ATM-dependent branch of the senescence response [146–148]. This is an attractive explanation, given recent evidence that ultra-low CBR in a DUL environment reduces ATM expression, and that ATM restoration partially rescues the associated cellular phenotype [149]. ATM is not merely a component of replicative senescence, but rather a major upstream determinant. ATM inhibition delays replicative senescence, reduced ATM responsiveness extends proliferative lifespan by increasing tolerance to dysfunctional telomeres [150], and ATM loss can bypass replication stress-induced senescence by attenuating DDR signaling while restoring the metabolic support for DNA synthesis [146,151]. In this framework, the selective reduction of palbociclib-induced senescence under DUL conditions may reflect the greater dependence of this senescence trajectory on an ATM-controlled replication surveillance axis. Reduced ATM abundance or signaling competence in cosmic silence would raise the threshold for full senescence engagement, allowing a subset of cells to evade or fail to consolidate the senescent state. Conversely, other forms of TIS may rely on damage inputs or effector circuits that are less ATM-dependent and therefore remain comparatively resistant to partial ATM attenuation. Additionally, ATM suppression restores vacuolar ATPase dimerization and steady-state lysosomal pH to enhance the autophagy-lysosome pathway function [152–154]. The latter phenomenon has been reported under growth stress in low-radiation DUL conditions, which could alleviate senescence phenotypes [155]. Together, the convergence between DUL-induced ATM downregulation and ATM's established role in replication stress-associated senescence provides a parsimonious explanation for why palbociclib-induced senescence, rather than senescence in general, is selectively vulnerable to the muon-less DUL environment. This mechanism remains to be tested directly in future LSC-DUL expeditions.

Cells deprived of the radiation noise from ionizing muonic tracks may undergo subtle shifts in the thresholds and signal-to-noise calibration that govern how they sense, interpret, and respond to damage and self-reinforcing feedback. Such maladaptive resetting could increase basal molecular damage while paradoxically weakening its conversion into the high-fidelity signaling amplitude required to cross the threshold for irreversible commitment to SA-β-gal-positive senescence. Longitudinal experiments in which cells are maintained in the DUL for months and then briefly re-primed with surface-level background radiation, or with calibrated low-dose ionizing radiation, as well as protocols that cycle cohorts between the DUL and the surface, could help determine whether this proposed loss of calibration remains reversible after long-term underground accommodation or instead becomes stably fixed. Available evidence from DUL studies suggests that cellular responses to deep-underground, low-background-radiation environments are both time- and cell type-dependent. In short-term experiments, measurable responses can arise quickly. Non-cancer hamster fibroblast V79 cells show distinct transcriptomic remodeling after only 2 days underground, and both V79

cells and FD-LSC-1 laryngeal squamous carcinoma cells exhibit reduced proliferation together with coordinated changes in redox pathways, RNA processing, ribosome/spliceosome programs, and organelle homeostasis within 2-4 days of underground culture [156–159]. Over a somewhat longer interval, V79 fibroblasts maintained for 23 days under below-background conditions displayed reduced viability beginning on day 5, suggesting that early molecular response can progress into sustained phenotypic divergence over subsequent weeks [160]. By contrast, older focused on much longer exposures, maintaining V79 fibroblasts for 9-10 months and TK6 lymphoblastoid cells for 6 months. These studies generally reported modest effects on bulk growth but reproducible changes in antioxidant defenses, stress responsiveness and mutation-related endpoints, consistent with chronic remodeling of cellular homeostasis under prolonged sub-background radiation conditions [161–164]. Similarly, long-term culture of human hybrid CGL1 cells for 16 weeks, with measurements every 4 weeks, revealed few changes in growth, survival, or basal DNA damage, yet showed progressively increased alkaline phosphatase activity, suggesting that transformation-related phenotypes may emerge even when conventional viability endpoints remain comparatively stable [165]. More recently, NP69 nasopharyngeal epithelial cells cultured underground showed reduced proliferation and migration over 36-96 h, together with transcriptomic enrichment in extracellular-matrix remodeling and post-transcriptional regulatory programs [166]. Within this framework, our 9–16-day underground culture window lies in an informative intermediate range between the acute responses observed during the first few days and the more stabilized phenotypes seen after weeks or months underground. This interval may therefore be particularly well-suited to resolving the transition from early stress sensing to longer-term compensatory adaptation.

To further address adaptation to reduced damage cells caused by diminished muon exposure, and the timescales over which such adaptation occurs, we are developing an evolutionary computational model. The model contains two basic components: a heterogeneous cell population, where each cell is defined by a damage threshold (DT), and an external damage level (DE) imposed on the population. The model's dynamics rest on two assumptions. First, transition to cell-cycle arrest or senescence occurs randomly when DE exceeds DT; the probability of arrest increases as DE rises further above DT. Second, cells that do not arrest continue to proliferate, but incur a fitness cost that penalizes low damage thresholds. This reflects the metabolic burden of maintaining damage-response machinery when external damage is low. This framework will allow us to test how and whether cells adapt to prevailing damage levels. After a shift in DE, we can also test how rapidly the population adapts to the new regime and how drugs or other physiological perturbations modify that process. One possible outcome is that the G0/G1 arrest trajectory results in a more heterogeneous distribution of how close individual senescent cells are to the SA-β-gal-positivity threshold within TIS populations. This makes the regulatory role of muons more easily detectable inside the DUL. However, our current approach cannot distinguish changes in cell-state fraction from changes in per-cell intensity. This approach employed mRNA-focused RNA-seq at the cell population (sample) level and whole SASP profiling in extracellular environments. Thus, testing whether DUL environmental conditions chiefly alter commitment heterogeneity or state depth would require multi-omics at the single-cell level across G0/G1 and G2/M arrest trajectories, ideally in clonal fibroblasts and oncogene-induced senescence systems [125, 167–171].

The previously unrecognized role of muons in regulating some aspects of the senescence response supports the idea that modern mammalian cells can sense background cosmic rays as part of their defense mechanisms. Our results are consistent with –and build upon– earlier work suggesting that natural radiation at Earth's surface acts as a constant, low-level stressor that prepares cells to respond quickly to sudden damage. When apoptosis or senescence is not efficiently activated, the absence of this priming may allow the damage to propagate further [125,164,172]. Human cancer cells appear to retain a vestigial, muon-tuned damage checkpoint that becomes evident in the absence of this abiotic calibrator even during short periods of cosmic silence. Based on these observations, one might speculate that G0/G1-like senescent trajectories, which require a continuum of cell-cycle withdrawal and could commonly operate in replicative aging, have evolutionarily exploited the omnipresent muon flux of CBR as a radiobiological gauge of replication fidelity. This process would spare cells that are merely proliferatively arrested, as quiescent cells in this path represent a reversible intermediate between proliferation and senescence. This allows apoptosis or senescence programs to eliminate or stably contain damaged cells in response to low-to-middle intensity damage. The G2/M pathway rapidly commits to and ensures senescence irrespective of the ambient muon background to preserve cellular and tissue integrity in response to a high-intensity damage that compromises genomes during cell division. Palbociclib serves as a tractable pharmacological proxy for the first pathway, whereas alisertib and bleomycin recapitulate the second pathway, which is crisis-like and dominated by mitotic and DNA damage stress. From a basic biology perspective, our findings suggest that natural CBR is a

hidden physiological cofactor that maintains genomic surveillance by fine-tuning senescence programs, rather than merely being a hazard. We acknowledge that these results further dispute the traditional linear no-threshold (LNT) model of radiation dose-damage risk [173–177].

Muons are produced in large quantities on Earth when primary cosmic rays interact with the atmosphere. In addition to ionizing the atmosphere, the secondary, high-energy muons generated in the air showers reach the ground and contribute to surface exposure. Muons are the most penetrating form of ionizing radiation and dominate the dose at ground level [177]. Therefore, although our findings should not be viewed as claims of altered organismal physiology in space but rather as specific, testable predictions about the senescence commitment barrier derived from our AGL-to-DUL delta analysis, they could have implications for habitats with low muon counts, such as the Moon and subsurface Mars (Fig. 11B) [178]. Lunar environments with negligible atmospheric pion production, and Martian habitats buried under meters of regolith to mitigate meteorite and high-energy hadron hazards recreate a DUL-like scarcity of muons. Our data suggest that the commitment to senescence in tissue repair, developmental growth arrest, tumor suppression, and other functions, may be altered depending on the path followed by the primary arrest stimuli. If our mechanism-informed and exploratory findings are mechanistically validated, two translational avenues for space and aging biomedicine emerge. On the one hand, we should identify tissues or drugs whose function or safety relies on muon-tuned senescence, safeguarded them, and retune them in extraterrestrial settings. This could involve localized "radiobiological priming" using tightly titrated, low-dose proton-beam "muon generators" or alternative abiotic stress analogs that can restore the fidelity of physiologically relevant senescence trajectories without incurring harmful doses. On the other hand, if our findings extend to a significant impact of cosmic silence on replicative senescence onset in the aging process, earlier studies showing that reduced CBR favors lifespan extension over reproductive output might be revisited under the lens of CBR-regulated functional senescence *in vivo* [179].

Our findings are subject to significant limitations that will require dedicated future campaigns at the LSC-DUL, as the logistical complexity of deep-underground facilities precludes immediate iteration with new experiments. First, a major limitation of the current study is the use of a transformed epithelial cell lines rather than primary non-transformed human cells. A549 cells were deliberately selected for this pilot study because our primary aim to determine whether DUL conditions can differentially reshape mechanistically distinct senescence programs in a controlled human cellular background. A549 cells have several advantages for this initial approach. They are a well-established lung epithelial/type II alveolar-like model that retains wild-type *TP53* and an inducible p53-p21 response. They have also been extensively validated as a senescence-competent system in response to diverse stressors [60,89,99–102]. Notably, A549 cells were among the core models used to develop the elastic-net SENCAN senescence classifier, where A549 senescent cells were used to train a transcriptomic predictor that subsequently generalized beyond cancer cells, correctly classifying several normal senescent fibroblasts and endothelial samples, while also discriminating senescence from quiescence in A549 cells. Furthermore, senescent phenotypes in cancer cells are highly context-dependent, often influenced as much by cellular lineage and genetic background as much as by the inducing stimulus itself. Using a single, well-characterized A549 background therefore enabled us to compare multiple senescence modalities while minimizing confounding factors such as donor variability, baseline replicative capacity, and the heterogeneous stress sensitivity of primary cultures. In fact, using a transformed but senescence-competent background provides conservative proof of the principle that any DUL-dependent modulation detected in A549 cells is unlikely to arise from the intrinsic fragility of primary cultures alone. In this study, A549 cells are not a definitive surrogate for healthy human tissues, but rather as a reproducible experimental platform to reveal whether the DUL environment selectively affects particular senescent trajectories (e.g., palbociclib-driven senescence). However, validation in primary epithelial and stromal models is necessary to determine the extent to which this selectively applies to non-transformed backgrounds. Second, we did not conduct *in situ* rescue experiments within the DUL by reintroducing precisely measured "CBR mimetics" (e.g., ultra-low dose protons or helium ions) during palbociclib treatment. This would have allowed us to determine whether restoring a muon-like term could recross the SA-β-gal barrier causally. Implementing titratable radiation "spikes" together with H2AX/ATM kinetics and real-time lysosomal readouts would provide stringent mechanistic validation. Third, relying on SA-β-gal as a late senescence marker raises the question of whether muon depletion directly alters lysosomal mass or acidification. A significant decrease in the oxidative tone of DUL cultures could result in fewer lysosomes acidifying enough to hydrolyze X-gal, although this scenario seems implausible because it would affect all TIS inducers equally. However, one could argue that this peculiarity is particularly relevant when using lysosomotropic drugs such as palbociclib, because their senescence-driving activity may partially depend on lysosome content and expansion [142,180–182]. Complementary LysoTracker or C12-FGD flow

cytometry, together with lysosomal biogenesis reporters, could determine whether palbociclib's sensitivity to distinct radiobiological environments is dictated by the distinct behavior of the lysosomal compartment. Additionally, we did not perform palbociclib "wash" experiments (palbociclib withdrawal) to test whether the reduced fraction of SA-β-gal positive cell at the DUL truly reflects a less severe, potentially reversible senescent state, rather than a simply delay in acquiring the SA-β-gal phenotype. Although SA-β-gal quantifications were robust, with large cell counts and multiple technical replicates, the logistical constraints of underground work limited the sample size (n=2), the range of assays, and number of time points. Thus, despite the stringent matching and monitoring of AGL/DUL experimental conditions, the findings from our hypothesis-generating study should be viewed as largely descriptive and exploratory. They must be replicated in longer campaigns at the LSC-DUL and in other independent DUL facilities worldwide before a definitive causal relationship can be established between CBR and the control of senescence programs in human cells can be established.

Conclusion

In conclusion, this exploratory study provides initial evidence that deep-underground, muon-depleted conditions do not disrupt senescence globally, but may subtly modulate the consolidation of specific senescence trajectories, most evidently those associated with G0/G1-targeted cell cycle withdrawal. The overall preservation of proliferative arrest, SENCAN scores and the general structure of the SASP argues against a complete reprogramming of senescence in cosmic silence. However, the palbociclib-biased effects suggest a certain degree of senescence sensitivity to muon depletion that depends on stress nature (replicative) and trajectory (G0/G1). These findings should be interpreted cautiously given the hypothesis-generating nature of the study, and replication and mechanistic validation are required across longer exposures, additional cell systems, and independent DUL facilities. If confirmed, they would support the view that CBR has acted as an overlooked environmental parameter in the evolutionary tuning of senescence programs. More broadly, DUL-based studies could provide a useful experimental framework for investigating how senescence operates in extraterrestrial environments lacking Earth's muon flux and examining the effects of cosmic silence on aging.

Acknowledgments

The authors acknowledge the environmental radiobiological characterization data, as well as the technical advice, which was provided within the framework of the collaboration between the Canfranc Underground Laboratory and the LABAC (University of Zaragoza). The schematics in Figures. 1, 2, 3, 7, 8, and 11 were created using BioRender.com.

The work in the Javier A. Menendez laboratory is supported by the Ministerio de Ciencia e Innovación and the Spanish Research Agency (MCIN/AEI, grant PID2022-141955OB-I00, Plan Nacional de I+D+i, funded by MCIN/AEI/10.13039/501100011033/ FEDER/ UE "ERDF A way of making Europe" funded by the European Regional Development Fund), and the Emerging Research Group SGR 2021 01507 of the Agència de Gestió d'Ajuts Universitaris i de Recerca (AGAUR, Generalitat de Catalunya). Elisabet Cuyàs holds a "Miguel Servet" research contract (CP20/00003) from the Instituto de Salud Carlos III (Spain) and is supported by the grant PI22/00297 (Instituto de Salud Carlos III, Proyectos de I+D+I en Salud, Acción Estratégica en Salud 2021–2023, funded by the "ERDF A way of making Europe"). Tomás Alarcón has been funded by grants PID2021-127896OB-I00 and PID2024-162434OB-I00 funded by MCIN/AEI/10.13039/ 501100011033 "ERDF A way of making Europe". This work has been funded also by the Spanish Research Agency (AEI) through the Severo Ochoa and Maria de Maeztu Program for Centers and Units of Excellence in R&D (CEX2020-001084-M). Javier A. Menendez, Tomás Alarcón, and Elisabet Cuyàs thank the CERCA Program/Generalitat de Catalunya for the institutional support.

Author contributions

ÀL-H: Methodology, Investigation, Validation, Data Curation, Formal analysis, Visualization. JL: Methodology, Investigation, Validation, Data Curation, Formal analysis, Visualization. SV: Conceptualization, Methodology, Validation, Data Curation, Formal analysis, Visualization. RH-A: Investigation, Resources, Supervision, Methodology. LC-B: Investigation, Resources, Supervision, Methodology. CP-G: Conceptualization, Project administration, Resources, Supervision, Writing–original draft; TA: Conceptualization, Resources, Supervision, Methodology, Visualization, Writing–original draft, Writing– review & editing. EC: Conceptualization, Project administration, Supervision, Resources, Methodology, Formal analysis, Visualization, Writing–original draft, Writing– review & editing. JAM: Conceptualization, Project administration, Supervision, Resources, Methodology, Formal analysis, Visualization, Writing–original draft, Writing– review & editing.

Data availability

All of the data sets used in the present study are available from the corresponding authors upon reasonable request. RNAseq data can be found in the NCBI Gene Expression Omnibus (GEO) database (www.ncbi.nlm.nih.gov/geo) under the accession number GSE310137.

Competing interest

All of the authors declare that they have no known competing financial interests or personal relationships that could appear to have influenced the work reported in this paper.

Ethics approval and consent to participate

All methods were performed in accordance with the relevant guidelines and regulations. None of the experiments in this study involved the use of materials (i.e., human or mouse samples) that are subject to ethical approval.

Consent for publication

All authors agreed to the publication of the article. All data were in-house and no paper mills were used. To ensure integrity and accuracy, all authors agree to take responsibility for all aspects of the work.

Supplementary Materials

The Supplementary data are avaibale online at: www.aginganddisease.org/EN/10.14336/AD.2026.0025.

References

[1] Antelo-Iglesias L, Picallos-Rabina P, Estévez-Souto V, Da Silva-Álvarez S, Collado M (2021). The role of cellular senescence in tissue repair and regeneration. Mech Ageing Dev, 198:111528.

[2] Campisi J, d'Adda di Fagagna F (2007). Cellular senescence: when bad things happen to good cells. Nat Rev Mol Cell Biol, 8:729–740.

[3] Collado M, Serrano M (2010). Senescence in tumours: evidence from mice and humans. Nat Rev Cancer, 10:51–57.

[4] Gil J (2025). The interplay between senescence, inflammation, and the immune system. Genes Dev, 39:923–925.

[5] Gorgoulis V, Adams PD, Alimonti A, Bennett DC, Bischof O, Bishop C, et al. (2019). Cellular Senescence: Defining a Path Forward. Cell, 179:813–827.

[6] Herranz N, Gil J (2018). Mechanisms and functions of cellular senescence. J Clin Invest, 128:1238–1246.

[7] Muñoz-Espín D, Serrano M (2014). Cellular senescence: from physiology to pathology. Nat Rev Mol Cell Biol, 15:482–496.

[8] Childs BG, Gluscevic M, Baker DJ, Laberge R-M, Marquess D, Dananberg J, et al. (2017) Senescent cells: an emerging target for diseases of ageing. Nat Rev Drug Discov, 16:718–735.

[9] Di Micco R, Krizhanovsky V, Baker D, d'Adda di Fagagna F (2021). Cellular senescence in ageing: from mechanisms to therapeutic opportunities. Nat Rev Mol Cell Biol, 22:75–95.

[10] López-Otín C, Blasco MA, Partridge L, Serrano M, Kroemer G (2023). Hallmarks of aging: An expanding universe. Cell, 186:243–278.

[11] Van Deursen JM (2014). The role of senescent cells in ageing. Nature, 509:439–446.

[12] Belyi VA, Ak P, Markert E, Wang H, Hu W, Puzio-Kuter A, et al. (2010). The Origins and Evolution of the p53 Family of Genes. Cold Spring Harb Perspect Biol, 2:a001198–a001198.

[13] Ciccia A, Elledge SJ (2010). The DNA Damage Response: Making It Safe to Play with Knives. Mol Cell, 40:179–204.

[14] Cussiol JRR, Soares BL, Oliveira FMB (2019). From yeast to humans: Understanding the biology of DNA Damage Response (DDR) kinases. Genet Mol Biol, 43(suppl 1):e20190071.

[15] Da Silva-Álvarez S, Picallos-Rabina P, Antelo-Iglesias L, Triana-Martínez F, Barreiro-Iglesias A, Sánchez L, et al. (2019). The development of cell senescence. Exp Gerontol, 128:110742.

[16] Harper JW, Elledge SJ (2007). The DNA Damage Response: Ten Years After. Mol Cell, 28:739–745.

[17] Kowald A, Passos JF, Kirkwood TBL (2020). On the evolution of cellular senescence. Aging Cell, 19:e13270.

[18] Chen H-A, Ho Y-J, Mezzadra R, Adrover JM, Smolkin R, Zhu C, et al. (2023) Senescence Rewires Microenvironment Sensing to Facilitate Antitumor Immunity. Cancer Discov, 13:432–453.

[19] Coppé J-P, Desprez P-Y, Krtolica A, Campisi J (2010). The Senescence-Associated Secretory Phenotype: The Dark Side of Tumor Suppression. Annu Rev Pathol Mech Dis, 5:99–118.

[20] Romesser PB, Lowe SW (2023). The Potent and Paradoxical Biology of Cellular Senescence in Cancer. Annu Rev Cancer Biol, 7:207–228.

[21] Wang B, Han J, Elisseeff JH, Demaria M (2024). The senescence-associated secretory phenotype and its physiological and pathological implications. Nat Rev Mol Cell Biol, 25:958–978.

[22] Basisty N, Kale A, Jeon OH, Kuehnemann C, Payne T, Rao C, et al. (2020). A proteomic atlas of senescence-associated secretomes for aging biomarker development. Serrano M, editor. PLOS Biol, 18:e3000599.

[23] Coppé J-P, Patil CK, Rodier F, Krtolica A, Beauséjour CM, Parrinello S, et al. (2010). A Human-Like Senescence-Associated Secretory Phenotype Is Conserved in Mouse Cells Dependent on Physiological Oxygen. PLoS One, 5:e9188.

[24] Da Silva-Álvarez S, Guerra-Varela J, Sobrido-Cameán D, Quelle A, Barreiro-Iglesias A, Sánchez L, et al. (2020). Cell senescence contributes to tissue regeneration in zebrafish. Aging Cell, 19:e13052.

[25] Ma X, Ding Y, Mondaca-Ruff D, Zhang X, Lu Y, Yoon B, et al. (2025). Nothobranchius furzeri: a vertebrate model for studying cardiac aging and cellular senescence. npj Aging, 11:63.

[26] Özcan S, Alessio N, Acar MB, Mert E, Omerli F, Peluso G, et al. (2016). Unbiased analysis of senescence associated secretory phenotype (SASP) to identify common components following different genotoxic stresses. Aging (Albany NY), 8:1316–1329.

[27] Ajoolabady A, Pratico D, Bahijri S, Tuomilehto J, Uversky VN, Ren J. (2025) Hallmarks of cellular senescence: biology, mechanisms, regulations. Exp Mol Med, 57:1482–1491.

[28] Huna A, Massemin A, Makulyte G, Flaman J-M, Martin N, Bernard D. (2024). Regulation of cell function and identity by cellular senescence. J Cell Biol, 223:e202401112.

[29] Ohtani N, Hara E (2013). Roles and mechanisms of cellular senescence in regulation of tissue homeostasis. Cancer Sci, 104:525–530.

[30] Reimann M, Lee S, Schmitt CA (2024). Cellular senescence: Neither irreversible nor reversible. J Exp Med, 221:e20232136.

[31] Varela-Eirín M, Demaria M (2022). Cellular senescence. Curr Biol, 32:R448–R452.

[32] Collado M, Gil J, Efeyan A, Guerra C, Schuhmacher AJ, Barradas M, et al. (2005). Tumor biology: senescence in premalignant tumours. Nature, 436:642.

[33] Marin I, Boix O, Garcia-Garijo A, Sirois I, Caballe A, Zarzuela E, et al. (2023). Cellular Senescence Is Immunogenic and Promotes Antitumor Immunity. Cancer Discov, 13:410–431.

[34] Serrano M, Lin AW, McCurrach ME, Beach D, Lowe SW (1997). Oncogenic ras Provokes Premature Cell Senescence Associated with Accumulation of p53 and p16INK4a. Cell, 88:593–602.

[35] Xue W, Zender L, Miething C, Dickins RA, Hernando E, Krizhanovsky V, et al. (2007). Senescence and tumour clearance is triggered by p53 restoration in murine liver carcinomas. Nature, 445:656–660.

[36] Demaria M, Ohtani N, Youssef SA, Rodier F, Toussaint W, Mitchell JR, et al. (2014). An Essential Role for Senescent Cells in Optimal Wound Healing through Secretion of PDGF-AA. Dev Cell, 31:722–733.

[37] Hernandez-Gonzalez F, Prats N, Ramponi V, López-Domínguez JA, Meyer K, Aguilera M, et al. (2023). Human senescent fibroblasts trigger progressive lung fibrosis in mice. Aging (Albany NY), 15:6641–6657.

[38] Mansfield L, Ramponi V, Gupta K, Stevenson T, Mathew AB, Barinda AJ, et al. (2024). Emerging insights in senescence: pathways from preclinical models to therapeutic innovations. npj Aging, 10:53.

[39] Maus M, López-Polo V, Mateo L, Lafarga M, Aguilera M, De Lama E, et al. (20239. Iron accumulation drives fibrosis, senescence and the senescence-associated secretory phenotype. Nat Metab, 5:2111–2130.

[40] Mavrogonatou E, Pratsinis H, Papadopoulou A, Karamanos NK, Kletsas D. (2019). Extracellular matrix alterations in senescent cells and their significance in tissue homeostasis. Matrix Biol, 75–76:27–42.

[41] Moiseeva V, Cisneros A, Sica V, Deryagin O, Lai Y, Jung S, et al. (2023). Senescence atlas reveals an aged-like inflamed niche that blunts muscle regeneration. Nature, 613:169–178.

[42] Oubaha M, Miloudi K, Dejda A, Guber V, Mawambo G, Germain M-A, et al. (2016). Senescence-associated secretory phenotype contributes to pathological angiogenesis in retinopathy. Sci Transl Med, 8:362ra144.

[43] Muñoz-Espín D, Cañamero M, Maraver A, Gómez-López G, Contreras J, Murillo-Cuesta S, et al. (2013). Programmed Cell Senescence during Mammalian Embryonic Development. Cell, 155:1104–1118.

[44] Storer M, Mas A, Robert-Moreno A, Pecoraro M, Ortells MC, Di Giacomo V, et al. (2013). Senescence Is a Developmental Mechanism that Contributes to Embryonic Growth and Patterning. Cell, 155:1119–1130.

[45] Zhao H, Liu Z, Chen H, Han M, Zhang M, Liu K, et al. (2024). Identifying specific functional roles for senescence across cell types. Cell, 187:7314–7334.

[46] Yun MH, Davaapil H, Brockes JP (2015). Recurrent turnover of senescent cells during regeneration of a complex structure. Elife, 4:e05505.

[47] Yu Q, Walters HE, Pasquini G, Pal Singh S, Lachnit M, Oliveira CR, et al. (2023). Cellular senescence promotes progenitor cell expansion during axolotl limb regeneration. Dev Cell, 58:2416–2427.

[48] Salinas-Saavedra M, Febrimarsa, Krasovec G, Horkan HR, Baxevanis AD, Frank U (2023). Senescence-induced cellular reprogramming drives cnidarian whole-body regeneration. Cell Rep, 42:112687.

[49] Walters HE, Troyanovskiy KE, Graf AM, Yun MH (2023). Senescent cells enhance newt limb regeneration by promoting muscle dedifferentiation. Aging Cell, 22:e13826.

[50] Chiche A, Le Roux I, von Joest M, Sakai H, Aguín SB, Cazin C, et al. (2017). Injury-Induced Senescence Enables In Vivo Reprogramming in Skeletal Muscle. Cell Stem Cell, 20:407–414.

[51] Rhinn M, Ritschka B, Keyes WM (2019). Cellular senescence in development, regeneration and disease. Development, 146:dev151837.

[52] Ring NAR, Valdivieso K, Grillari J, Redl H, Ogrodnik M (2022). The role of senescence in cellular plasticity: Lessons from regeneration and development and implications for age-related diseases. Dev Cell, 57:1083–1101.

[53] Antoniou A, Pharoah PDP, Narod S, Risch HA, Eyfjord JE, Hopper JL, et al. (2003). Average Risks of Breast and Ovarian Cancer Associated with BRCA1 or BRCA2 Mutations Detected in Case Series Unselected for Family History: A Combined Analysis of 22 Studies. Am J Hum Genet, 72:1117–1130.

[54] Walters HE, Yun MH (2020). Rising from the ashes: cellular senescence in regeneration. Curr Opin Genet Dev, 64:94–100.
[55] Baker DJ, Wijshake T, Tchkonia T, LeBrasseur NK, Childs BG, van de Sluis B, et al. (2011). Clearance of p16Ink4a-positive senescent cells delays ageing-associated disorders. Nature, 479:232–236.
[56] Colucci M, Sarill M, Maddalena M, Valdata A, Troiani M, Massarotti M, et al. (2025). Senescence in cancer. Cancer Cell, 43:1204–1226.
[57] He S, Sharpless NE (2017). Senescence in Health and Disease. Cell, 169:1000–1011.
[58] Huang W, Hickson LJ, Eirin A, Kirkland JL, Lerman LO (2022). Cellular senescence: the good, the bad and the unknown. Nat Rev Nephrol, 18:611–627.
[59] Schmitt CA, Wang B, Demaria M (2022). Senescence and cancer — role and therapeutic opportunities. Nat Rev Clin Oncol, 19:619–636.
[60] Baz-Martínez M, Da Silva-Álvarez S, Rodríguez E, Guerra J, El Motiam A, Vidal A, et al. (2016). Cell senescence is an antiviral defense mechanism. Sci Rep, 6:37007.
[61] Kohli J, Veenstra I, Demaria M (2021). The struggle of a good friend getting old: cellular senescence in viral responses and therapy. EMBO Rep, 22:e52243.
[62] Kim JH, Brown SL, Gordon MN (2023). Radiation-induced senescence: therapeutic opportunities. Radiat Oncol, 18:10.
[63] von Zglinicki T (2024). Oxidative stress and cell senescence as drivers of ageing: Chicken and egg. Ageing Res Rev, 102:102558.
[64] Victorelli S, Passos JF (2017). Telomeres and Cell Senescence - Size Matters Not. EBioMedicine, 21:14–20.
[65] Xue-Ling L, Ding J, Ling-Hua M (2018). Oncogene-induced senescence: a double edged sword in cancer. Acta Pharmacol Sin, 39:1553–1558.
[66] Hewitt G, Jurk D, Marques FDM, Correia-Melo C, Hardy T, Gackowska A, et al. (2012). Telomeres are favoured targets of a persistent DNA damage response in ageing and stress-induced senescence. Nat Commun, 3:708.
[67] D'Adda Di Fagagna F (2008). Living on a break: Cellular senescence as a DNA-damage response. Nat Rev Cancer, 8:512–522.
[68] Belli M, Indovina L (2020). The Response of Living Organisms to Low Radiation Environment and Its Implications in Radiation Protection. Front Public Heal, 8:601711.
[69] de Groen PC (2022). Muons, mutations, and planetary shielding. Front Astron Sp Sci, 9:1067491.
[70] Allkofer OC, Carstensen K, Dau WD (1971). The absolute cosmic ray muon spectrum at sea level. Phys Lett B, 36:425–427.
[71] Allkofer OC, Dau WD, Jokisch H, Klemke G, Uhr RC, Bella G, et al. (1985). Primary-cosmic-ray energy spectrum up to 50 TeV derived from sea-level muon measurements. Phys Rev D, 31:1557–1560.
[72] Thorne MC (2003). Background radiation: natural and man-made. J Radiol Prot, 23:29–42.
[73] Rastegarzadeh G, Khoshabadi S (2016). Measurement of muon production depth in cosmic ray induced extensive air showers by time structure of muons at observation level. New Astron, 44:45–50.
[74] Laubenstein M, Lawson I (2020). Low Background Radiation Detection Techniques and Mitigation of Radioactive Backgrounds. Front Phys, 8:577734.
[75] UNSCEAR. Source and effects of ionizing radiation United Nations scientific committee on the effects of Atomic Radiation UNSCEAR 2000 Report to General Assembly with Scientific Annexes. Vol. Volume I, United Nations. 2000.
[76] Liu J, Ma T, Liu Y, Zou J, Gao M, Zhang R, et al. (2018). History, advancements, and perspective of biological research in deep-underground laboratories: A brief review. Environ Int, 120:207–114.
[77] Zou Y, Wang L, Wen J, Cheng J, Li C, Hao Z, et al. (2023). Progress in biological and medical research in the deep underground: an update. Front Public Heal, 11:1249742.
[78] Ianni A (2021). Science in Underground Laboratories and DULIA-Bio. Front Phys, 9:611146.
[79] Pérez-Pérez J, Amare JC, Bandac IC, Bayo A, Borjabad-Sánchez S, Calvo-Mozota JM, et al. (2022). Radon Mitigation Applications at the Laboratorio Subterráneo de Canfranc (LSC). Universe, 8:112.
[80] Bandac I, Borjabad S, Ianni A, Nuñez-Lagos R, Pérez C, Rodríguez S, et al. (2017). Ultra-low background and environmental measurements at Laboratorio Subterráneo de Canfranc (LSC). Appl Radiat Isot, 126:127–129.
[81] Hernández-Antolín R, Cid-Barrio L, Peña-Garay C (2024). Canfranc biology platform: exploring life in cosmic silence. Front Phys, 12:1397799.
[82] Ewald JA, Desotelle JA, Wilding G, Jarrard DF (2010). Therapy-Induced Senescence in Cancer. JNCI J Natl Cancer Inst, 102:1536–1546.
[83] Prasanna PG, Citrin DE, Hildesheim J, Ahmed MM, Venkatachalam S, Riscuta G, et al. (2021). Therapy-Induced Senescence: Opportunities to Improve Anticancer Therapy. JNCI J Natl Cancer Inst, 113:1285–1298.
[84] Wang L, Lankhorst L, Bernards R (2022). Exploiting senescence for the treatment of cancer. Nat Rev Cancer, 22:340–355.
[85] Wang L, Bernards R (2018). Taking advantage of drug resistance, a new approach in the war on cancer. Front Med, 12:490–495.
[86] Santos-de-Frutos K, Djouder N (2021). When dormancy fuels tumour relapse. Commun Biol, 4:747.
[87] Bajtai E, Kiss C, Bakos É, Langó T, Lovrics A, Schád É, et al. (2025). Therapy-induced senescence is a transient drug resistance mechanism in breast cancer. Mol Cancer, 24:128.
[88] Saleh T, Greenberg EF, Faber AC, Harada H, Gewirtz DA (2025). A Critical Appraisal of the Utility of Targeting Therapy-Induced Senescence for Cancer Treatment. Cancer Res, 85:1755–1768.
[89] Jochems F, Thijssen B, De Conti G, Jansen R, Pogacar Z, Groot K, et al. (2021). The Cancer SENESCopedia: A

delineation of cancer cell senescence. Cell Rep, 36:109441.
[90] Wang B, Varela-Eirin M, Brandenburg SM, Hernandez-Segura A, van Vliet T, Jongbloed EM, et al. (2022). Pharmacological CDK4/6 inhibition reveals a p53-dependent senescent state with restricted toxicity. EMBO J, 41:e108946–e108946.
[91] Lee DH, Imran M, Choi JH, Park YJ, Kim YH, Min S, et al. (2024). CDK4/6 inhibitors induce breast cancer senescence with enhanced anti-tumor immunogenic properties compared with DNA-damaging agents. Mol Oncol, 18:216–232.
[92] Trzaska WH, Slupecki M, Bandac I, Bayo A, Bettini A, Bezrukov L, et al. (2019). Cosmic-ray muon flux at Canfranc Underground Laboratory. Eur Phys J C, 79:721.
[93] Plaza J, Martínez T, Bécares V, Cano-Ott D, Villamarín D, Pérez de Rada A, et al. (2023). Thermal neutron background at Laboratorio Subterráneo de Canfranc (LSC). Astropart Phys, 146:102793.
[94] Kim D, Langmead B, Salzberg SL (2015). HISAT: a fast spliced aligner with low memory requirements. Nat Methods, 12:357–360.
[95] Pertea M, Pertea GM, Antonescu CM, Chang TC, Mendell JT, Salzberg SL (2015). StringTie enables improved reconstruction of a transcriptome from RNA-seq reads. Nat Biotechnol, 33:290–295.
[96] Love MI, Huber W, Anders S (2014). Moderated estimation of fold change and dispersion for RNA-seq data with DESeq2. Genome Biol, 15:550.
[97] Raudvere U, Kolberg L, Kuzmin I, Arak T, Adler P, Peterson H, et al. (2019). g:Profiler: a web server for functional enrichment analysis and conversions of gene lists (2019 update). Nucleic Acids Res, 47:W191–Q198.
[98] Chen EY, Tan CM, Kou Y, Duan Q, Wang Z, Meirelles GV, et al. (2013). Enrichr: interactive and collaborative HTML5 gene list enrichment analysis tool. BMC Bioinformatics, 14:128.
[99] Tesei A, Arienti C, Bossi G, Santi S, De Santis I, Bevilacqua A, et al. (2021). TP53 drives abscopal effect by secretion of senescence-associated molecular signals in non-small cell lung cancer. J Exp Clin Cancer Res, 40:89.
[100] Aoshiba K, Tsuji T, Nagai A (2003). Bleomycin induces cellular senescence in alveolar epithelial cells. Eur Respir J, 22:436–443.
[101] López J, Llop-Hernández À, Verdura S, Serrano-Hervás E, Martinez-Balibrea E, Bosch-Barrera J, et al. (2025). Mitochondrial priming and response to BH3 mimetics in "one-two punch" senogenic-senolytic strategies. Cell Death Discov, 11:91.
[102] Tsuji T, Aoshiba K, Nagai A (2004). Cigarette Smoke Induces Senescence in Alveolar Epithelial Cells. Am J Respir Cell Mol Biol, 31:643–649.
[103] Wagner V, Gil J (2020). Senescence as a therapeutically relevant response to CDK4/6 inhibitors. Oncogene, 39:5165–5176.
[104] Wang L, Leite de Oliveira R, Wang C, Fernandes Neto JM, Mainardi S, Evers B, et al. (2017). High-Throughput Functional Genetic and Compound Screens Identify Targets for Senescence Induction in Cancer. Cell Rep, 21:773–783.
[105] Vilgelm AE, Johnson CA, Prasad N, Yang J, Chen S-C, Ayers GD, et al. (2016). Connecting the Dots: Therapy-Induced Senescence and a Tumor-Suppressive Immune Microenvironment. JNCI J Natl Cancer Inst, 108:djv406.
[106] Do T-V, Hirst J, Hyter S, Roby KF, Godwin AK (2017). Aurora A kinase regulates non-homologous end-joining and poly(ADP-ribose) polymerase function in ovarian carcinoma cells. Oncotarget, 8:50376–50392.
[107] Hirst J, Godwin AK (2017). AURKA inhibition mimics BRCAness. Aging (Albany NY), 9:1945–1946.
[108] Povirk LF (1996). DNA damage and mutagenesis by radiomimetic DNA-cleaving agents: bleomycin, neocarzinostatin and other enediynes. Mutat Res - Fundam Mol Mech Mutagen, 355:71–89.
[109] Regulus P, Duroux B, Bayle P-A, Favier A, Cadet J, Ravanat J-L (2007). Oxidation of the sugar moiety of DNA by ionizing radiation or bleomycin could induce the formation of a cluster DNA lesion. Proc Natl Acad Sci, 104:14032–14037.
[110] Lu T, Zhang Y, Kidane Y, Feiveson A, Stodieck L, Karouia F, et al. (2017). Cellular responses and gene expression profile changes due to bleomycin-induced DNA damage in human fibroblasts in space. Chuang EY, editor. PLoS One, 12:e0170358.
[111] Low EK, Brudvik E, Kuhlman B, Wilson PF, Almeida-Porada G, Porada CD (2018). Microgravity Impairs DNA Damage Repair in Human Hematopoietic Stem/Progenitor Cells and Inhibits Their Differentiation into Dendritic Cells. Stem Cells Dev, 27:1257–1267.
[112] Llop-Hernández À, Verdura S, López J, Martin-Castillo B, Menendez JA, Cuyàs E. Mitochondrial bioenergetics-SASP crosstalk determines senolytic efficacy in therapy-induced senescence. Cell Death Discov, 2026;12:103.
[113] Lee BY, Han JA, Im JS, Morrone A, Johung K, Goodwin EC, et al. (2006). Senescence-associated β-galactosidase is lysosomal β-galactosidase. Aging Cell, 5:187–195.
[114] Debacq-Chainiaux F, Erusalimsky JD, Campisi J, Toussaint O (2009). Protocols to detect senescence-associated beta-galactosidase (SA-βgal) activity, a biomarker of senescent cells in culture and in vivo. Nat Protoc, 4:1798–1806.
[115] Tan JX, Finkel T (2023). Lysosomes in senescence and aging. EMBO Rep, 24:e57265.
[116] Maskey RS, Wang F, Lehman E, Wang Y, Emmanuel N, Zhong W, et al. (2021). Sustained mTORC1 activity during palbociclib-induced growth arrest triggers senescence in ER+ breast cancer cells. Cell Cycle, 20:65–80.
[117] Afifi MM, Crncec A, Cornwell JA, Cataisson C, Paul D, Ghorab LM, et al. (2023). Irreversible cell cycle exit associated with senescence is mediated by constitutive MYC degradation. Cell Rep, 42:113079.
[118] Kudo R, Safonov A, Jones C, Moiso E, Dry JR, Shao H, et al. (2024). Long-term breast cancer response to CDK4/6 inhibition defined by TP53-mediated geroconversion. Cancer Cell, 42:1983.
[119] Hong T, Hogger AC, Wang D, Pan Q, Gansel J, Engleitner T, et al. (2024). CDK4/6 inhibition initiates

cell cycle arrest by nuclear translocation of RB and induces a multistep molecular response. Cell Death Discov, 10:453.
[120] Casella G, Munk R, Kim KM, Piao Y, De S, Abdelmohsen K, et al. (2019). Transcriptome signature of cellular senescence. Nucleic Acids Res, 47:7294–7305.
[121] Mahmud S, Pitcher LE, Torbenson E, Robbins PD, Zhang L, Dong X. (2024). Developing transcriptomic signatures as a biomarker of cellular senescence. Ageing Res Rev, 99:102403.
[122] Frey Y, Haj M, Ziv Y, Elkon R, Shiloh Y (2025). Broad repression of DNA repair genes in senescent cells identified by integration of transcriptomic data. Nucleic Acids Res, 53:gkae1257.
[123] Chan M, Yuan H, Soifer I, Maile TM, Wang RY, Ireland A, et al. (2022). Novel insights from a multiomics dissection of the Hayflick limit. Elife, 11:e70283.
[124] Stallaert W, Taylor SR, Kedziora KM, Taylor CD, Sobon HK, Young CL, et al. (2022). The molecular architecture of cell cycle arrest. Mol Syst Biol, 18:e11087.
[125] Evans SA, Voan Teo Y, Hinthorn SJ, Clark K, Ito T, Sedivy JM, et al. (2023). Single-Cell Transcriptomics Reveals Global Markers of Transcriptional Diversity across Different Forms of Cellular Senescence. Aging Biol, 1:20230008.
[126] Fernandez B, Passanisi VJ, Ashraf HM, Spencer SL (2025). Single-cell RNA sequencing reveals a quiescence-senescence continuum and distinct senotypes following chemotherapy. Nat Commun, 17:169.
[127] Farfariello V, Iamshanova O, Germain E, Fliniaux I, Prevarskaya N (2015). Calcium homeostasis in cancer: A focus on senescence. Biochim Biophys Acta - Mol Cell Res, 1853:1974–1979.
[128] Warnier M, Flaman J, Chouabe C, Wiel C, Gras B, Griveau A, et al. (2018). The SCN9A channel and plasma membrane depolarization promote cellular senescence through Rb pathway. Aging Cell, 17:e12736.
[129] Jeffries EP, Di Filippo M, Galbiati F (2019). Failure to reabsorb the primary cilium induces cellular senescence. FASEB J, 33:4866–4882.
[130] Chen A, Jin J, Cheng S, Liu Z, Yang C, Chen Q, et al. (2022). mTORC1 induces plasma membrane depolarization and promotes preosteoblast senescence by regulating the sodium channel Scn1a. Bone Res, 10:25.
[131] Li M, Gong W, Chen J, Zhang Y, Ma Y, Tu X (2023). PPP3R1 Promotes MSCs Senescence by Inducing Plasma Membrane Depolarization and Increasing Ca2+ Influx. Int J Mol Sci, 24:4421.
[132] Ma X, Zhang Y, Zhang Y, Zhang X, Huang Y, He K, et al. (2023). A stress-induced cilium-to-PML-NB route drives senescence initiation. Nat Commun, 14:1840.
[133] Protasoni M, López-Polo V, Stephan-Otto Attolini C, Brandariz J, Herranz N, Mateo J, et al. (2024). Cyclophilin D plays a critical role in the survival of senescent cells. EMBO J, 43:5972–6000.
[134] Sediqi H, Levin M (2025). Bioelectric characterization of senescing human keratinocytes. iScience, 28:113275.
[135] Milanovic M, Fan DNY, Belenki D, Däbritz JHM, Zhao Z, Yu Y, et al. (2018). Senescence-associated reprogramming promotes cancer stemness. Nature, 553:96–100.
[136] Evangelou K, Belogiannis K, Papaspyropoulos A, Petty R, Gorgoulis VG. (2023). Escape from senescence: molecular basis and therapeutic ramifications. J Pathol, 260:649–665.
[137] O'Sullivan EA, Wallis R, Mossa F, Bishop CL (2024). The paradox of senescent-marker positive cancer cells: challenges and opportunities. npj Aging, 10:41.
[138] Pusalkar S, Zhou X, Li Y, Cohen L, Yang JJ, Balani SK, et al. (2020). Biotransformation Pathways and Metabolite Profiles of Oral [^{14}C]Alisertib (MLN8237), an Investigational Aurora A Kinase Inhibitor, in Patients with Advanced Solid Tumors. Drug Metab Dispos, 48:217–229.
[139] Azizieh F, Dingle K, Raghupathy R, Johnson K, VanderPlas J, Ansari A (2018). Multivariate analysis of cytokine profiles in pregnancy complications. Am J Reprod Immunol, 79:e12818.
[140] Dingle K, Kassem OM, Azizieh F, AbdulHussain G, Raghupathy R (2023). Quantitative analyses of cytokine profiles reveal hormone-mediated modulation of cytokine profiles in recurrent spontaneous miscarriage. Cytokine, 164:156160.
[141] Crozier L, Foy R, Mouery BL, Whitaker RH, Corno A, Spanos C, et al. (2022). CDK4/6 inhibitors induce replication stress to cause long-term cell cycle withdrawal. EMBO J, 41:e108599.
[142] Nehme J, Maassen S, Bravaccini S, Zanoni M, Gianni C, De Giorgi U, et al. (2025). Pharmacological CDK4/6 inhibition promotes vulnerability to lysosomotropic agents in breast cancer. EMBO J, 44:1921–1942.
[143] Xiong J, Zhu MX (2016). Regulation of lysosomal ion homeostasis by channels and transporters. Sci China Life Sci, 59:777–791.
[144] López-Hernández T, Puchkov D, Krause E, Maritzen T, Haucke V (2020). Endocytic regulation of cellular ion homeostasis controls lysosome biogenesis. Nat Cell Biol, 22:815–827.
[145] Gerasimenko J V, Gerasimenko O V, Petersen OH (2001). Membrane repair: Ca 2+ -elicited lysosomal exocytosis. Curr Biol, 11:R971–R974.
[146] Aird KM, Worth AJ, Snyder NW, Lee JV, Sivanand S, Liu Q, et al. (2015). ATM couples replication stress and metabolic reprogramming during cellular senescence. Cell Rep, 11:893-901.
[147] Aird KM, Zhang R (2015). ATM in senescence. Oncotarget, 6:14729–14730.
[148] Stagni V, Ferri A, Cirotti C, Barilà D (2021). ATM Kinase-Dependent Regulation of Autophagy: A Key Player in Senescence? Front Cell Dev Biol, 8:599048.
[149] Ma T, Wen J, Li S, Li C, Wang L, Hao Z, et al. (2026). Ultra-low background radiation inhibits head and neck tumor via ATM downregulation mediated mitochondrial dysfunction. Cancer Lett, 636:218138.
[150] Stuart AJ, Takai KK, Gabbasova RR, Sanford H, Vinogradova EV, de Lange T (2025). Attenuation

of ATM signaling by ROS delays replicative senescence at physiological oxygen. Mol Cell, 85:4667–4677.
[151] Pandey SN, Afzal M, Uikey J, Ganesan S, Mishra S, Bansal P, et al. (2025). ATM and p53 in aging and cancer: a double-edged sword in genomic integrity. Biogerontology, 26:102.
[152] Kang HT, Park JT, Choi K, Kim Y, Choi HJC, Jung CW, et al. (2017). Chemical screening identifies ATM as a target for alleviating senescence. Nat Chem Biol, 13:616–623.
[153] Kwon Y, Kim JW, Jeoung JA, Kim MS, Kang C (2017). Autophagy Is Pro-Senescence When Seen in Close-Up, but Anti-Senescence in Long-Shot. Mol Cells, 40:607–612.
[154] Kuk MU, Kim JW, Lee YS, Cho KA, Park JT, Park SC (2019). Alleviation of Senescence via ATM Inhibition in Accelerated Aging Models. Mol Cells, 42:210–217.
[155] Fischietti M, Fratini E, Verzella D, Vecchiotti D, Capece D, Di Francesco B, et al. (2021). Low Radiation Environment Switches the Overgrowth-Induced Cell Apoptosis Toward Autophagy. Front Public Heal, 8:594789.
[156] Liu J, Ma T, Gao M, Liu Y, Liu J, Wang S, et al. (2020). Proteomics provides insights into the inhibition of Chinese hamster V79 cell proliferation in the deep underground environment. Sci Rep, 10:14921.
[157] Liu J, Ma T, Gao M, Liu Y, Liu J, Wang S, et al. (2020) Proteomic Characterization of Proliferation Inhibition of Well-Differentiated Laryngeal Squamous Cell Carcinoma Cells Under Below-Background Radiation in a Deep Underground Environment. Front Public Health, 8:584964.
[158] Duan L, Jiang H, Liu J, Liu Y, Ma T, Xie Y, et al. (2021). Whole Transcriptome Analysis Revealed a Stress Response to Deep Underground Environment Conditions in Chinese Hamster V79 Lung Fibroblast Cells. Front Genet, 12:698046.
[159] Liu Y, Gao Y, Cheng J, Ma T, Xie Y, Wen Q, et al. (2022). Transcriptome analysis of well-differentiated laryngeal squamous cell carcinoma cells in below-background environment. Ann Transl Med, 10:824.
[160] Castillo H, Winder J, Smith G (2022). Chinese hamster V79 cells' dependence on background ionizing radiation for optimal growth. Radiat Environ Biophys, 61:49–57.
[161] Antonelli F, Belli M, Sapora O, Simone G, Sorrentino E, Tabocchini MA, et al. (2000) Radiation biophysics at the Gran Sasso laboratory: influence of a low background radiation environment on the adaptive response of living cells. Nucl Phys B (Proceedings Supplements), 87: 508–509.
[162] Satta L, Antonelli F, Belli M, Sapora O, Simone G, Sorrentino E, et al. (2002). Influence of a low background radiation environment on biochemical and biological responses in V79 cells. Radiat Environ Biophys, 41:217–224.
[163] Carbone MC, Pinto M, Antonelli F, Amicarelli F, Balata M, Belli M, et al. (2009). The Cosmic Silence experiment: on the putative adaptive role of environmental ionizing radiation. Radiat Environ Biophys, 48:189–196.
[164] Fratini E, Carbone C, Capece D, Esposito G, Simone G, Tabocchini MA, et al. (2015) Low-radiation environment affects the development of protection mechanisms in V79 cells. Radiat Environ Biophys, 54:183–194.
[165] Pirkkanen J, Laframboise T, Peterson J, Labelle A, Mahoney F, Lapointe M, et al. (2024). The Role of Natural Background Radiation in Maintaining Genomic Stability in the CGL1 Human Hybrid Model System. Radiat Res, 202:617–625.
[166] Hao Z, Li C, Wang L, Zou Y, Wen J, Wu J, et al. (2025) [Inhibitory Effects of the Deep Underground Low Background Radiation Environment on the Proliferation and Migration of NP69 Human Nasopharyngeal Epithelial Cells and the Underlying Mechanisms]. Sichuan Da Xue Xue Bao Yi Xue Ban, 56:1336–1343.
[167] Saul D, Kosinsky RL, Atkinson EJ, Doolittle ML, Zhang X, LeBrasseur NK, et al. (2022). A new gene set identifies senescent cells and predicts senescence-associated pathways across tissues. Nat Commun, 13:4827.
[168] Tao W, Yu Z, Han J-DJ (2024). Single-cell senescence identification reveals senescence heterogeneity, trajectory, and modulators. Cell Metab, 36:1126-1143.
[169] Sanborn MA, Wang X, Gao S, Dai Y, Rehman J (2025). Unveiling the cell-type-specific landscape of cellular senescence through single-cell transcriptomics using SenePy. Nat Commun,16:1884.
[170] Wang J, Zhou X, Yu P, Yao J, Guo P, Xu Q, et al. (2025). A transcriptome-based human universal senescence index (hUSI) robustly predicts cellular senescence under various conditions. Nat Aging, 5:1159–1175.
[171] Ito T, Teo YV, Evans SA, Neretti N, Sedivy JM (2018). Regulation of Cellular Senescence by Polycomb Chromatin Modifiers through Distinct DNA Damage- and Histone Methylation-Dependent Pathways. Cell Rep, 22:3480–3492.
[172] Morciano P, Cipressa F, Porrazzo A, Esposito G, Tabocchini MA, Cenci G. (2018). Fruit Flies Provide New Insights in Low-Radiation Background Biology at the INFN Underground Gran Sasso National Laboratory (LNGS). Radiat Res, 190:217.
[173] Esposito G, Anello P, Ampollini M, Bortolin E, De Angelis C, D'Imperio G, et al. (2020). Underground Radiobiology: A Perspective at Gran Sasso National Laboratory. Front Public Heal, 8:611146.
[174] Lampe N, Breton V, Sarramia D, Sime-Ngando T, Biron DG (2017). Understanding low radiation background biology through controlled evolution experiments. Evol Appl, 10:658–666.
[175] Wadsworth J, Cockell CS, Murphy AS, Nilima A, Paling S, Meehan E, et al. (2020). There's Plenty of Room at the Bottom: Low Radiation as a Biological Extreme. Front Astron Sp Sci, 7:50
[176] Zarubin M, Gangapshev A, Gavriljuk Y, Kazalov V, Kravchenko E. (2021). First transcriptome profiling of D. melanogaster after development in a deep underground low radiation background laboratory. PLoS One, 16:e0255066.

[177] Atri D, Melott A (2011). Biological implications of high-energy cosmic ray induced muon flux in the extragalactic shock model. Geophys Res Lett, 38:L19203.

[178] Leone G, Tanaka HKM, Holma M, Krishnan S, Duffy AR, Enqvist T, et al. (2025). Positioning, navigation, and timing on the Moon and Mars with galactic cosmic rays. iScience, 28:112496.

[179] Morciano P, Iorio R, Iovino D, Cipressa F, Esposito G, Porrazzo A, et al. (2018). Effects of reduced natural background radiation on Drosophila melanogaster growth and development as revealed by the FLYINGLOW program. J Cell Physiol, 233:23–29.

[180] Llanos S, Megias D, Blanco-Aparicio C, Hernández-Encinas E, Rovira M, Pietrocola F, et al. (2019). Lysosomal trapping of palbociclib and its functional implications. Oncogene, 38:3886–3902.

[181] Fassl A, Brain C, Abu-Remaileh M, Stukan I, Butter D, Stepien P, et al. (2020). Increased lysosomal biomass is responsible for the resistance of triple-negative breast cancers to CDK4/6 inhibition. Sci Adv, 6:eabb2210.

[182] Rovira M, Sereda R, Pladevall-Morera D, Ramponi V, Marin I, Maus M, et al. (2022). The lysosomal proteome of senescent cells contributes to the senescence secretome. Aging Cell, 21:e13707.